NASA Technical Memorandum 4118

A Hierarchy of Transport Approximations for High Energy Heavy (HZE) Ions

John W. Wilson
Langley Research Center
Hampton, Virginia

Barry D. Ganapol
University of Arizona
Tucson, Arizona

Stanley L. Lamkin
PRC Kentron, Inc.
Aerospace Technologies Division
Hampton, Virginia

Lawrence W. Townsend
Langley Research Center
Hampton, Virginia

Hamidullah Farhat
Hampton University
Hampton, Virginia

National Aeronautics and
Space Administration
Office of Management
Scientific and Technical
Information Division

1989

Contents

Abstract

The transport of high energy heavy (HZE) ions through bulk materials is studied with energy dependence of the nuclear cross sections being neglected. A three-term perturbation expansion appears to be adequate for most practical applications for which penetration depths are less than 30 g/cm^2 of material. The differential energy flux is found for monoenergetic beams and for realistic ion beam spectral distributions. An approximate formalism is given to estimate higher order terms.

1. Introduction

Although heavy ion transport codes for use in space applications are in a relatively advanced stage at Langley Research Center (refs. 1 through 3), it seems prudent to further develop the theory for comparison with laboratory experiments, which has been recently neglected since initial efforts began several years ago (refs. 4 through 7). In the present report, we begin with the most simplified assumptions for which the problem may be solved completely. Solutions to a more complete theory may then be compared with prior results as limiting cases. In this way, the more complete but approximate analysis will have some basis for evaluating the accuracy of the solution method. The lowest order approximation will be totally energy-independent. The most complicated solution to be considered herein will have energy-independent nuclear cross sections but will treat the energy-dependent atomic/molecular processes and the energy spread of the primary beam. A fully energy-dependent theory must await further development, although some terms have been previously evaluated (ref. 6).

2. Energy-Independent Flux

If the ion beam is of sufficiently high energy that the energy shift due to atomic/molecular collisions brings none of the particles to rest in the region of interest, then

$$\left[\frac{\partial}{\partial x} + \sigma_j\right] \phi_j(x) = \sum_k m_{jk}\sigma_k \, \phi_k(x) \tag{2.1}$$

where $\phi_j(x)$ is the flux of type j ions, σ_j is the nuclear absorption cross section, and m_{jk} is the fragmentation parameter for producing type j ions from type k. The solution for a given incident ion type J is given in terms of a set of g-functions as follows:

$$g(j_1) = \exp(-\sigma_{j_1} x) \tag{2.2}$$

$$g(j_1, j_2, \ldots, j_n, j_{n+1}) = \frac{g(j_1, j_2, \ldots, j_{n-1}, j_n) - g(j_1, j_2, \ldots, j_{n-1}, j_{n+1})}{\sigma_{jn+1} - \sigma_{jn}} \tag{2.3}$$

for which the solution for the type j ion flux is written as

$$\phi_j^{(0)}(x) = \delta_{J_j} \, g(j) \tag{2.4}$$

$$\phi_j^{(1)}(x) = m_{jJ}\sigma_J \, g(j, J) = m_{jJ}\sigma_J \frac{\exp(-\delta_j x) - \exp(-\delta_J x)}{\sigma_J - \sigma_j} \tag{2.5}$$

$$\phi_j^{(2)}(x) = \sum_k m_{jk}\sigma_k \, m_{kJ}\sigma_J \, g(j, k, J) \tag{2.6}$$

$$\phi_j^{(3)}(x) = \sum_{k,l} m_{jk}\sigma_k \, m_{kl}\sigma_l m_{lJ}\sigma_J \, g(j, k, l, J) \tag{2.7}$$

with

$$\phi_j(x) = \sum_i \phi_j^{(i)}(x) \tag{2.8}$$

This solution is equivalent to that derived by Ganapol et al. in reference 8. We now consider some applications of the above formalism. The cross-section data base is discussed elsewhere (ref. 9).

2.1. Neon Beam Transport

We first note in the case of ^{20}Ne incident on water that ^{19}Ne and ^{19}F have only one contributing term in equation (2.8). These are shown in figure 2.1. Also shown in figure 2.1

are the fluxes of various isotopes of secondary ion fragments. The effect of successive terms of equation (2.8) is shown in table 2.1 for the ^{15}O flux. It is clear from the table that the fourth and higher order collision terms are completely negligible and that third collision terms are a rather minor contribution. Hence, a three-term expansion as we have used in the past (refs. 5, 6, and 7) appears justified. The relative magnitude of the terms contributing to the ^{7}Li flux generated by the ^{20}Ne beam is presented in table 2.2. The fourth collision term is negligible at small penetration distances and small, but not negligible, at distances greater than 30 cm. The greater penetrating power of the lighter mass fragments is demonstrated in figure 2.2. Also note the difference in solution character due to the importance of the higher order term.

2.2. Iron Beam Transport

We first note in the case of ^{56}Fe incident on water that ^{55}Fe and ^{55}Mn have only one contributing term in equation (2.8). The ^{54}Mn has but two terms, and the slight difference in solution character can be seen in figure 2.3. Results for ^{52}V are also shown. The convergence rate of equation (2.8) is demonstrated in table 2.3. Again we see the fourth collision term to be negligible, whereas the three-term expansion we have used before seems quite accurate at these depths for these ions. In distinction to prior results, the ^{16}O flux has significant contributions from higher order terms for depths beyond 20 cm as seen in table 2.4. Clearly, a more complete theory using higher order terms is required than previously used for ion beams of particles heavier than ^{20}Ne. The different solution character of the lighter mass fragments is clearly demonstrated in figure 2.4.

Table 2.1. Normalized Contributions to ^{15}O Flux From Successive Collision Terms for ^{20}Ne Transport in Water

Fragment term	^{15}O flux at x of—				
	10 cm	20 cm	30 cm	40 cm	50 cm
$\phi^{(1)}$	1.00E0	1.00E0	1.00E0	1.00E0	1.00E0
$\phi^{(2)}$	1.01E-1	2.01E-1	3.02E-1	4.03E-1	5.04E-1
$\phi^{(3)}$	2.63E-3	1.05E-2	2.36E-2	4.18E-2	6.52E-2
$\phi^{(4)}$	3.31E-5	2.52E-4	8.58E-4	2.03E-3	3.95E-3

Table 2.2. Normalized Contributions to ^{7}Li Flux From Successive Collision Terms for ^{20}Ne Transport in Water

Fragment term	^{7}Li flux at x of—				
	10 cm	20 cm	30 cm	40 cm	50 cm
$\phi^{(1)}$	1.00E0	1.00E0	1.00E0	1.00E0	1.00E0
$\phi^{(2)}$	1.62E-1	3.20E-1	4.72E-1	6.18E-1	7.58E-1
$\phi^{(3)}$	1.15E-2	4.53E-2	9.98E-2	1.73E-1	2.63E-1
$\phi^{(4)}$	4.02E-4	3.16E-3	1.04E-2	2.39E-2	4.53E-2

Table 2.3. Normalized Contributions to ^{52}V Flux From Successive Collision Terms for ^{56}Fe Transport in Water

Fragment term	^{52}V flux at x of—				
	10 cm	20 cm	30 cm	40 cm	50 cm
$\phi^{(1)}$	1.00E0	1.00E0	1.00E0	1.00E0	1.00E0
$\phi^{(2)}$	7.91E-2	1.52E-1	2.37E-1	3.15E-1	3.94E-1
$\phi^{(3)}$	2.37E-3	9.48E-3	2.13E-2	3.79E-2	5.91E-2
$\phi^{(4)}$	2.24E-5	1.73E-4	5.93E-4	1.41E-3	2.75E-3

Table 2.4. Normalized Contributions to ^{16}O Flux From Successive Collision Terms for ^{56}Fe Transport in Water

Fragment term	^{16}O flux at x of—				
	10 cm	20 cm	30 cm	40 cm	50 cm
$\phi^{(1)}$	1.00E0	1.00E0	1.00E0	1.00E0	1.00E0
$\phi^{(2)}$	5.87E-1	1.12E0	1.59E0	2.00E0	2.36E0
$\phi^{(3)}$	1.86E-1	7.08E-1	1.49E0	2.46E0	3.56E0
$\phi^{(4)}$	3.06E-2	2.63E-1	9.44E-1	2.33E0	4.72E0

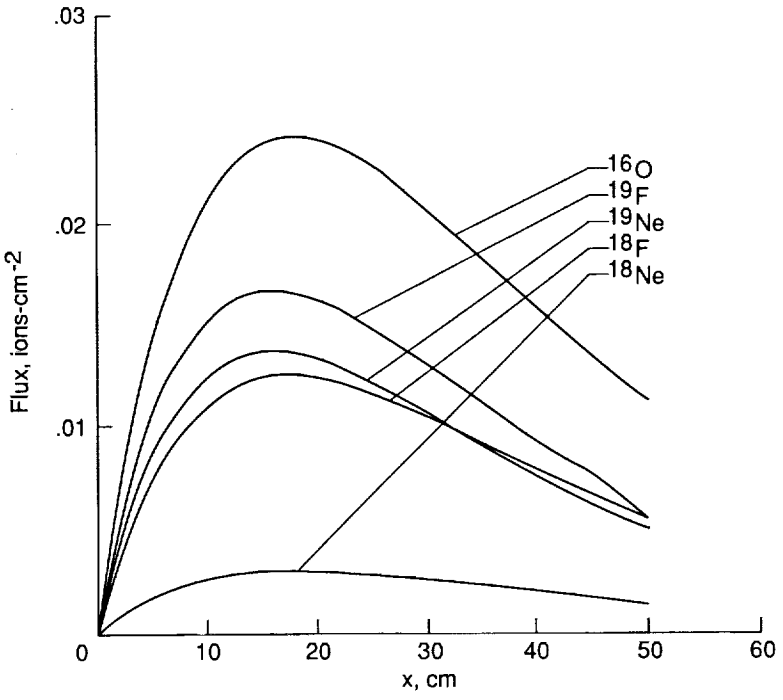

Figure 2.1. Ion fragment flux of various isotopes as a function of depth in water for a ^{20}Ne incident beam.

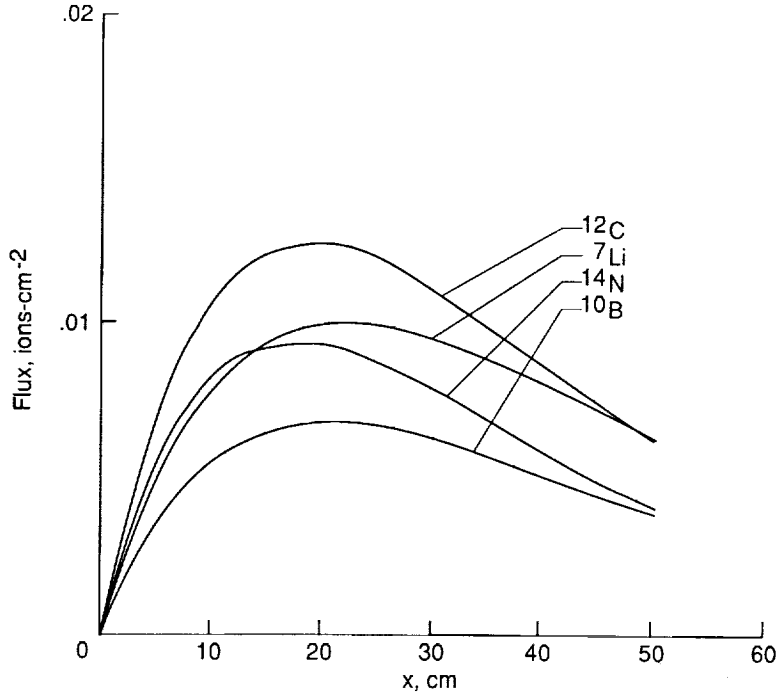

Figure 2.2. Flux of light ion fragments as a function of depth in water for a ^{20}Ne incident beam.

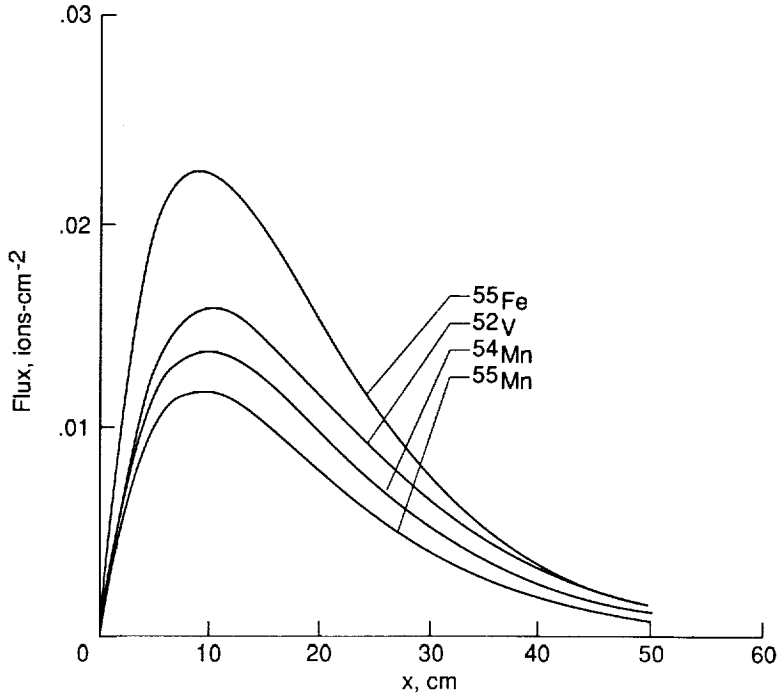

Figure 2.3. Ion fragment flux of various isotopes as a function of depth in water for a ^{56}Fe incident beam.

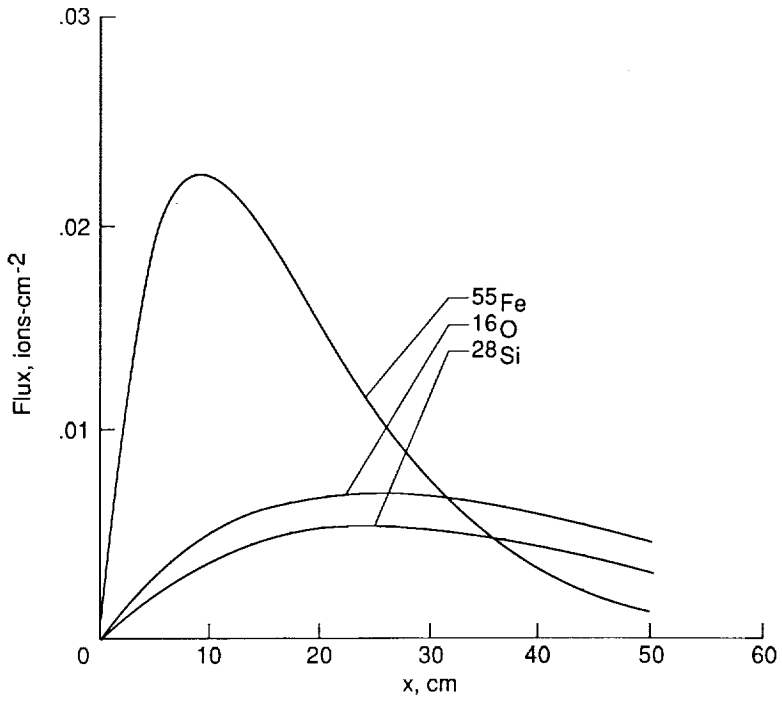

Figure 2.4. Flux of light ion fragments as a function of depth in water for a ^{56}Fe incident beam.

3. Monoenergetic Ion Beams

In moving through extended matter, heavy ions lose energy through interaction with atomic electrons along their trajectories. On occasion, they interact violently with nuclei of the matter and produce ion fragments moving in the forward direction and low energy fragments of the struck target nucleus. The transport equations for the short range target fragments can be solved in closed form in terms of collision density (refs. 5 and 6). Hence, the projectile fragment transport is the interesting unsolved problem. In previous work, the projectile ion fragments were treated as if all went straightforward (ref. 4). We continue with this assumption herein, noting that an extension of the beam fragmentation model to three dimensions is being developed (ref. 9).

With the straightahead approximation and the target secondary fragments neglected (refs. 4, 5, and 6), the transport equation may be written as

$$\left[\frac{\partial}{\partial x} - \frac{\partial}{\partial E}\widetilde{S}_j(E) + \sigma_j\right] \phi_j(x,E) = \sum_{k>j} m_{jk}\sigma_k \, \phi_k(x,E) \tag{3.1}$$

where $\phi_j(x,E)$ is the flux of ions of type j with atomic mass A_j at x moving along the x-axis at energy E in units of MeV/amu, σ_j is the corresponding macroscopic nuclear absorption cross section, $\widetilde{S}_j(E)$ is the change in E per unit distance, and m_{jk} is the fragmentation parameter for ion j produced in collision by ion k. The range of the ion is given as

$$R_j(E) = \int_0^E \frac{dE'}{\widetilde{S}_j(E')} \tag{3.2}$$

The stopping powers used herein are based on Ziegler's fits to a large data base (refs. 11 through 16). There is some controversy as to the stopping powers to be used (ref. 10). The analysis in reference 10 was biased to the stopping power used in the data analysis and is the same as that used in the PROPAGATE code. The values in the HZESEC computer code are similar to those in PROPAGATE. Neither the PROPAGATE nor HZESEC stopping powers

have been compared with the data base collected by Ziegler as far as is known to us. We continue to use Ziegler's work until more definitive comparisons compel us to do otherwise.

The solution to equation (3.1) is to be found subject to boundary specification at $x = 0$ and arbitrary E as

$$\phi_j(0, E) = F_j(E) \tag{3.3}$$

Usually $F_j(E)$ is called the incident beam spectrum.

It follows from Bethe's theory that

$$\tilde{S}_j(E) = \frac{A_p Z_j^2}{A_j Z_p^2} \tilde{S}_p(E) \tag{3.4}$$

for which

$$\frac{Z_j^2}{A_j} R_j(E) = \frac{Z_p^2}{A_p} R_p(E) \tag{3.5}$$

The subscript p refers to proton. Equation (3.5) is quite accurate at high energy and only approximately true at low energy because of electron capture by the ion which effectively reduces its charge, higher order Born corrections to Bethe's theory, and nuclear stopping at the lowest energies. Herein, the parameter ν_j is defined as

$$\nu_j = \frac{Z_j^2}{A_j} \tag{3.6}$$

so that

$$\nu_j \; R_j(E) = \nu_k \; R_k(E) \tag{3.7}$$

Equations (3.6) and (3.7) are used in the subsequent development, and the energy variation in ν_j is neglected. The inverse function of $R_j(E)$ is defined as

$$E = R_j^{-1} \left[R_j(E) \right] \tag{3.8}$$

and plays a fundamental role subsequently. For the purpose of solving equation (3.1), define the coordinate transformation (refs. 5 and 6),

$$\left.\begin{aligned} \eta_j &\equiv x - R_j(E) \\ \xi_j &\equiv x + R_j(E) \end{aligned}\right\} \tag{3.9}$$

and new functions

$$\left.\begin{aligned} \chi_j(\eta_j, \xi_j) &\equiv \tilde{S}_j(E) \; \phi_j(x, E) \\ \overline{\chi}_k(\eta_j, \xi_j) &\equiv \chi_k(\eta_k, \xi_k) \end{aligned}\right\} \tag{3.10}$$

where

$$\left.\begin{aligned} \xi_j + \eta_j &= \xi_k + \eta_k \\ \eta_j - \xi_j &= \frac{\nu_k}{\nu_j}(\eta_k - \xi_k) \end{aligned}\right\} \tag{3.11}$$

for which equation (3.1) becomes

$$\left(2\frac{\partial}{\partial \eta_j} + \sigma_j \right) \chi_j(\eta_j, \xi_j) = \sum_k \; m_{jk} \sigma_k \frac{\nu_j}{\nu_k} \; \overline{\chi}_k(\eta_j, \xi_j) \tag{3.12}$$

where the σ_j is assumed to be energy independent. Solving equation (3.12) by using line integration with the integrating factor,

$$\mu_j(\eta_j, \xi_j) = \exp\left[\frac{1}{2}\sigma_j(\xi_j + \eta_j)\right] \tag{3.13}$$

results in

$$\chi_j(\eta_j, \xi_j) = \exp\left[-\frac{1}{2}\sigma_j(\xi_j + \eta_j)\right] \chi_j(-\xi_j, \xi_j)$$
$$+ \frac{1}{2}\int_{-\xi_j}^{\eta_j} \exp\left[\frac{1}{2}\sigma_j(\eta' - \eta_j)\right] \sum_k m_{jk}\sigma_k \frac{\nu_j}{\nu_k}\, \chi_k(\eta'_k, \xi'_k)\, d\eta' \tag{3.14}$$

where

$$\left.\begin{aligned} \eta'_k &= \frac{\nu_k + \nu_j}{2\nu_k}\eta' + \frac{\nu_k - \nu_j}{2\nu_k}\,\xi_j \\ \xi'_k &= \frac{\nu_k - \nu_j}{2\nu_k}\eta' + \frac{\nu_k + \nu_j}{2\nu_k}\xi_j \end{aligned}\right\} \tag{3.15}$$

and the boundary condition (eq. (3.3)) is written as

$$\chi_j(-\xi_j, \xi_j) = \tilde{S}_j\left[R_j^{-1}(\xi_j)\right]\; F_j\left[R_j^{-1}(\xi_j)\right]$$

Consider a Neumann series for equation (3.14) for which the first term is

$$\chi_j^{(0)}(\eta_j, \xi_j) = \exp\left[-\frac{1}{2}\sigma_j(\eta_j + \xi_j)\right]\; \tilde{S}_j\left[R_j^{-1}(\xi_j)\right]\; F_j\left[R_j^{-1}(\xi_j)\right] \tag{3.16}$$

and the second term is

$$\chi_j^{(1)}(\eta_j, \xi_j) = \frac{1}{2}\int_{-\xi_j}^{\eta_j} \exp\left[\frac{1}{2}\sigma_j(\eta' - \eta_j)\right] \sum_k m_{jk}\sigma_k \frac{\nu_j}{\nu_k} \exp\left[-\frac{1}{2}\sigma_k(\eta'_k - \xi'_k)\right]$$
$$\times\, \tilde{S}_k\left[R_k^{-1}(\xi'_k)\right]\; F_k\left[R_k^{-1}(\xi'_k)\right]\; d\eta' \tag{3.17}$$

An expression for $\chi_j^{(2)}(\eta_j, \xi_j)$ is derived once equation (3.17) is reduced and higher order terms can be found by continued iteration of equation (3.14). These expressions (eqs. (3.16) and (3.17)) are now simplified for a monoenergetic beam of type M ions.

The boundary condition is now taken as

$$F_j(E) = \delta_{jM}\; \delta(E - E_o) \tag{3.18}$$

where δ_{jM} is the Kronecker delta, $\delta(\;)$ is the Dirac delta, and E_o is the incident beam energy. Thus,

$$\chi_j(-\xi_j, \xi_j) = \tilde{S}_j\left[R_j^{-1}(\xi_j)\right]\; \delta_{jM}\; \delta\left[R_j^{-1}(\xi_j) - E_o\right] = \delta_{jM}\; \delta[\xi_j - R_j(E_o)] \tag{3.19}$$

for which $\chi_j^{(0)}$ becomes

$$\chi_j^{(0)}(\eta_j, \xi_j) = \delta_{jM} \exp\left[-\frac{1}{2}\sigma_j(\eta_j + \xi_j)\right]\; \delta[\xi_j - R_j(E_o)] \tag{3.20}$$

and $\chi_j^{(1)}$ becomes

$$\chi_j^{(1)}(\eta_j,\xi_j) = \frac{1}{2}\int_{-\xi_j}^{\eta_j} m_{jM}\sigma_M\frac{\nu_j}{\nu_M}\exp\left[\frac{1}{2}\sigma_j\eta_j - \frac{1}{2}\sigma_M(\eta'_M + \xi'_M)\right] \times \delta[\xi'_M - R_M(E_o)]\ d\eta' \tag{3.21}$$

where ξ'_M is given by equation (3.15) for $k = M$. The contribution to the integral (eq. (3.21)) occurs at

$$\eta' = \frac{2\nu_M}{\nu_M - \nu_j}\ R_M(E_o) - \frac{\nu_M + \nu_j}{\nu_M - \nu_j}\xi_j \tag{3.22}$$

provided that η' lies on the interval $-\xi_j < \eta' < \eta_j$ so that

$$\chi_j^{(1)}(\eta_j,\xi_j) = \frac{m_{jM}\sigma_M\nu_j}{|\nu_M - \nu_j|}\exp\left[-\frac{1}{2}\sigma_M(\xi_j + \eta') - \frac{1}{2}\sigma_j(\eta_j - \eta')\right] \tag{3.23}$$

The simplified form in equation (3.23) may now be used to calculate the next iteration of equation (3.14):

$$\chi_j^{(2)}(\eta_j,\xi_j) = \frac{1}{2}\sum_k m_{jk}\sigma_k m_{kM}\sigma_M\frac{\nu_j}{|\nu_M - \nu_k|}\int_{-\xi_j}^{\eta_j}\exp\left[-\frac{1}{2}\sigma_M(\xi''_k + \tilde{\eta}) - \frac{1}{2}\sigma_k(\eta''_k - \tilde{\eta}) - \frac{1}{2}\sigma_j(\eta_j - \eta'')\right] d\eta'' \tag{3.24}$$

where

$$\left.\begin{aligned}\eta''_k &= \frac{\nu_k + \nu_j}{2\nu_k}\eta'' + \frac{\nu_k - \nu_j}{2\nu_k}\xi_j\\ \xi''_k &= \frac{\nu_k - \nu_j}{2\nu_k}\eta'' + \frac{\nu_k + \nu_j}{2\nu_k}\xi_j\end{aligned}\right\} \tag{3.25}$$

and

$$\tilde{\eta} = \frac{2\nu_M}{\nu_M - \nu_k}\ R_M(E_o) - \frac{\nu_M + \nu_k}{\nu_M - \nu_k}\xi''_k \tag{3.26}$$

with the requirement that $-\xi''_k < \tilde{\eta} < \eta''_k$. The inverse of the transformation is now applied to obtain from equation (3.20)

$$\phi_j^{(0)}(x,E) = \frac{1}{\tilde{S}_j(E)}\exp(-\sigma_j x)\ \delta_{jM}\ \delta[x + R_j(E) - R_M(E_o)] \tag{3.27}$$

and from equation (3.23)

$$\phi_j^{(1)}(x,E) = \frac{1}{\tilde{S}_j(E)}m_{jM}\sigma_M\frac{\nu_j}{|\nu_M - \nu_j|}\exp\left\{-\frac{1}{2}\sigma_j\left[x - R_j(E) - \eta'\right] - \frac{1}{2}\sigma_M\left[x + R_j(E) + \eta'\right]\right\} \tag{3.28}$$

so long as

$$\frac{\nu_M}{\nu_j}\left[R_M(E_o) - x\right] < R_j(E) < \frac{\nu_M}{\nu_j}R_M(E_o) - x \tag{3.29}$$

Otherwise $\phi_j^{(1)}(x,E)$ is zero. After a complicated but straightforward manipulation, a similar result may be obtained from equation (3.24) for $\phi_j^{(2)}(x,E)$.

In reducing equation (3.24), it is useful to define

$$x_M = \frac{1}{2}\left(\xi_k'' + \tilde{\eta}\right) \tag{3.30}$$

$$x_k = \frac{1}{2}\left(\eta_k'' - \tilde{\eta}\right) \tag{3.31}$$

$$x_j = \frac{1}{2}\left(\eta_j - \eta''\right) \tag{3.32}$$

and make a change in variables as

$$\phi_j^{(2)}(x,E) = \frac{1}{\tilde{S}_j(E)} \sum_k m_{jk}\sigma_k m_{kM}\sigma_M \frac{\nu_j}{|\nu_M - \nu_k|} \int_{x_{jl}}^{x_{ju}} \exp(-\sigma_M x_M - \sigma_k x_k - \sigma_j x_j)\, dx_j \tag{3.33}$$

where the integral is understood to be nonzero only in the physically allowed regions as explained presently. One may easily demonstrate

$$x_M + x_k + x_j = x \tag{3.34}$$

$$\nu_M x_M + \nu_k x_k + \nu_j x_j = \nu_M\, R_M(E_o) - \nu_k\, R_k(E) \tag{3.35}$$

for which the parametric solution is given as

$$x_M = \frac{\nu_M\, R_M(E_o) - \nu_k[R_k(E) + x] + (\nu_k - \nu_j)x_j}{\nu_M - \nu_k} \tag{3.36}$$

$$x_k = \frac{\nu_M[R_M(E) + x] - \nu_M\, R_M(E_o) - (\nu_M - \nu_j)x_j}{\nu_M - \nu_k} \tag{3.37}$$

The requirement that x_M and x_k be bounded by the interval 0 to $x - x_j$ yields

$$\left\{ \begin{array}{c} 0 \\ \dfrac{\nu_k\,[R_k(E) + x] - \nu_M\, R_M(E_o)}{\nu_k - \nu_j} \end{array} \right\} \leq x_j \leq \left\{ \begin{array}{c} x \\ \dfrac{\nu_M\,[R_M(E) + x] - \nu_M\, R_M(E_o)}{\nu_M - \nu_j} \end{array} \right\} \tag{3.38}$$

as the appropriate limits for the integral in equation (3.33) when $\nu_M > \nu_k > \nu_j$. In the braces in equation (3.38), we always choose the most restrictive value for the limit. The requirement of equation (3.38) also implies the result that

$$R_M^{-1}\left[R_M(E_o) - x\right] \leq E \leq R_k^{-1}\left[\frac{\nu_M\, R_M(E_o) - \nu_j x}{\nu_k}\right] \tag{3.39}$$

as the range over which the result of equation (3.33) is not zero. In the event that $\nu_k > \nu_M > \nu_j$, then

$$\left\{ \begin{array}{c} 0 \\ \dfrac{\nu_M\,[R_M(E) + x] - \nu_M\, R_M(E_o)}{\nu_M - \nu_j} \end{array} \right\} \leq x_j \leq \left\{ \begin{array}{c} x \\ \dfrac{\nu_k\,[R_k(E) + x] - \nu_M\, R_M(E_o)}{\nu_k - \nu_j} \end{array} \right\} \tag{3.40}$$

As a result of equation (3.40)

$$R_k^{-1}\left[\frac{\nu_M}{\nu_k}\, R_M(E_o) - x\right] \leq E \leq R_M^{-1}\left[R_M(E_o) - \frac{\nu_j}{\nu_M} x\right] \tag{3.41}$$

In the event that $\nu_M > \nu_j > \nu_k$, it follows that

$$0 \leq x_j \leq \left\{ \begin{array}{c} x \\ \dfrac{\nu_M \left[R_M(E) + x - R_M(E_o)\right]}{\nu_M - \nu_j} \\ \dfrac{\nu_M R_M(E_o) - \nu_k \, R_k(E) - \nu_k x}{\nu_j - \nu_k} \end{array} \right\} \tag{3.42}$$

where the lesser of the three values in the braces is used as the upper limit of x_j for which the integral of equation (3.24) is not zero. As a result of equation (3.42)

$$R_M^{-1}\left[R_M(E_o) - x\right] \leq E \leq R_k^{-1}\left[\frac{\nu_M}{\nu_k} \, R_M(E_o) - x\right] \tag{3.43}$$

The integral in equation (3.33) may now be evaluated as

$$\phi_j^{(2)}(x,E) = \sum_k \frac{\sigma_{jk}\sigma_{kM}\nu_j}{\widetilde{S}_j(E)\,|\nu_M - \nu_k|\Delta_{jkM}} \left[\exp(-\sigma_M x_{Ml} - \sigma_k x_{kl} - \sigma_j x_{jl}) \right.$$

$$\left. - \exp(-\sigma_M x_{Mu} - \sigma_k x_{ku} - \sigma_j x_{ju})\right] \tag{3.44}$$

where x_{Mu}, x_{ku}, x_{Ml}, and x_{kl} are the values of equations (3.36) and (3.37) evaluated at the corresponding upper and lower limits of x_j and

$$\Delta_{jkM} = \sigma_j + \left[\frac{(\nu_k - \nu_j)}{(\nu_M - \nu_k)}\sigma_M - \frac{(\nu_M - \nu_j)}{(\nu_M - \nu_k)}\sigma_k\right] \tag{3.45}$$

Higher order terms are similarly derived.

The total integral flux associated with each term may be evaluated as

$$\Phi_j^{(1)}(x) = \int_o^\infty \phi_j^{(1)}(x,E)\, dE \tag{3.46}$$

One may easily show that

$$\int_0^\infty \phi_j^{(1)}(x,E)\, dE = \frac{\sigma_{jM}\left[\exp(-\sigma_j x) - \exp(-\sigma_M x)\right]}{\sigma_M - \sigma_j} \tag{3.47}$$

in agreement with equation (2.5). Furthermore

$$\int_0^\infty \phi_j^{(2)}(x,E)\, dE = \sum_k \frac{\sigma_{jk}\sigma_{kM}}{|\nu_M - \nu_k|\Delta_{jkM}} \left\{ \left(\frac{\nu_k - \nu_j}{\sigma_k - \sigma_j}\right)\left[\exp(-\sigma_j x) - \exp(-\sigma_k x)\right] \right.$$

$$\left. - \left(\frac{\nu_M - \nu_j}{\sigma_M - \sigma_j}\right)\left[\exp(-\sigma_j x) - \exp(-\sigma_M x)\right]\right\} \tag{3.48}$$

which agrees with equation (2.6) as $\nu_k \rightarrow \nu_M$. This relation of equation (3.48) and equation (2.6) has been used previously (ref. 7).

3.1. Total Flux Comparisons

The results of equations (3.28) and (3.44) are integrated numerically over their entire energy spectrum and given along with values from corresponding energy-independent solutions in

table 3.1. The primary beam was taken as ^{20}Ne at 1380 MeV/amu. Clearly, the energy-dependent solutions appear quite accurate.

3.2. Monoenergetic Beam Results

The fluorine spectral flux seen at various depths in a water column is shown in figure 3.1. The primary beam was ^{20}Ne ions at 600 MeV/amu corresponding to a range of 30 cm. There is a clear structure due to the fluorine isotopes shown in the spectrum. The most energetic ions are ^{19}F. The ^{18}F and ^{17}F spectral components are clearly resolved. Only the ^{19}F is able to penetrate to the largest depth represented (35 cm). A similar, but more complicated, isotopic structure is seen in the oxygen spectra of figure 3.2. The greater number of oxygen isotopes contributing has a smoothing effect on the resultant spectrum. This effect is even more clearly seen in figure 3.3 for the nitrogen isotopes. Some of the smoothness results from the higher order term $\phi^{(2)}$ in the perturbation expansion. The boron flux of figure 3.4 shows very little isotopic structure. Qualitatively, similar results are obtained for an iron beam of the same range (30 cm) as shown in figures 3.5 to 3.9.

Table 3.1. Total Flux From Energy-Independent Solution and Numerically Integrated Differential Spectrum

[Values in parentheses are from energy-independent solution]

Fragment	Term	Flux, cm^{-2}, at water depth x of—	
		5 cm	20 cm
^{18}F	$\phi^{(1)}$	0.00727 (0.00717)	0.01148 (0.01140)
	$\phi^{(2)}$	0.00018 (0.00018)	0.00114 (0.00114)
^{17}O	$\phi^{(1)}$	0.00729 (0.00729)	0.01173 (0.01174)
	$\phi^{(2)}$	0.00017 (0.00017)	0.00112 (0.00112)
^{16}O	$\phi^{(1)}$	0.01350 (0.01349)	0.02193 (0.02202)
	$\phi^{(2)}$	0.00029 (0.00029)	0.00191 (0.00190)
^{15}N	$\phi^{(1)}$	0.00470 (0.00481)	0.00796 (0.00796)
	$\phi^{(2)}$	0.00032 (0.00033)	0.00220 (0.00220)
^{13}C	$\phi^{(1)}$	0.00511 (0.00521)	0.00894 (0.00887)
	$\phi^{(2)}$	0.00032 (0.00033)	0.00224 (0.00224)
^{12}C	$\phi^{(1)}$	0.00668 (0.00682)	0.01173 (0.01178)
	$\phi^{(2)}$	0.00056 (0.00056)	0.00398 (0.00398)
^{11}B	$\phi^{(1)}$	0.00417 (0.00417)	0.00735 (0.00732)
	$\phi^{(2)}$	0.00036 (0.00036)	0.00259 (0.00259)

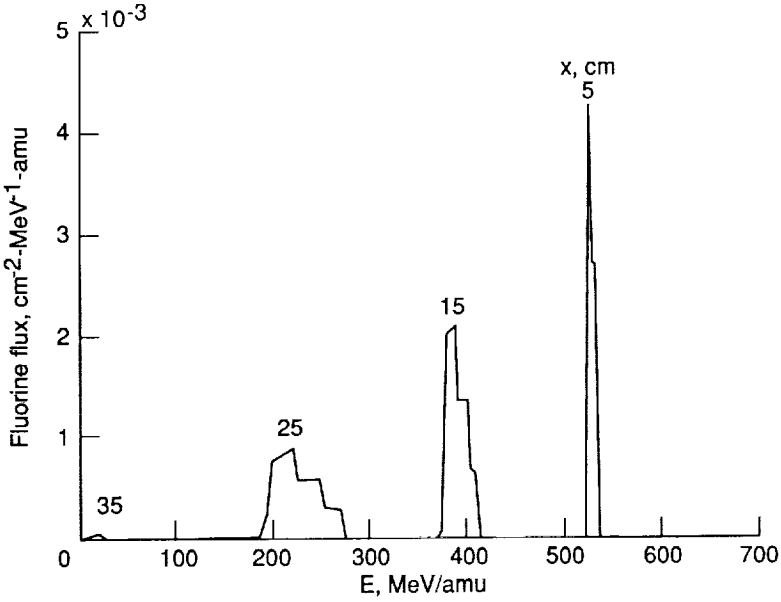

Figure 3.1. Fluorine flux spectrum produced by a ^{20}Ne beam at 600 MeV/amu in a water column at various depths.

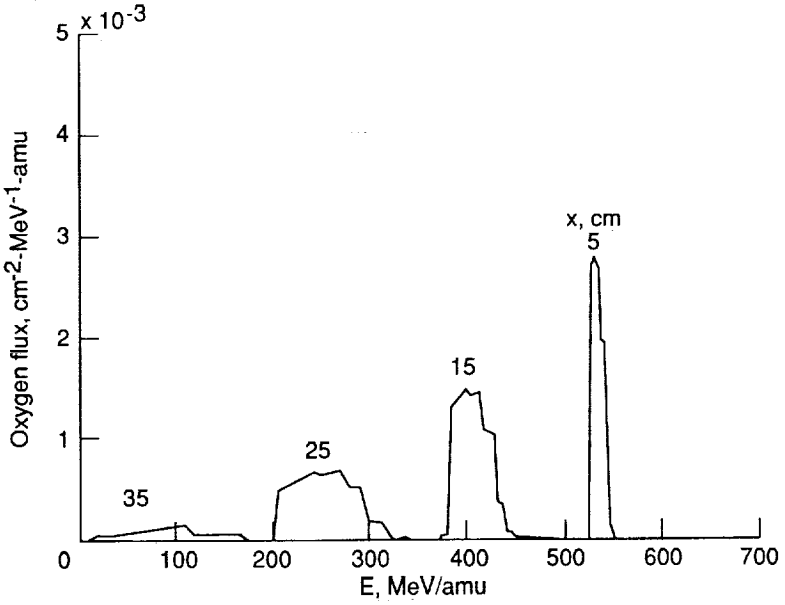

Figure 3.2. Oxygen flux spectrum produced by a ^{20}Ne beam at 600 MeV/amu in a water column at various depths.

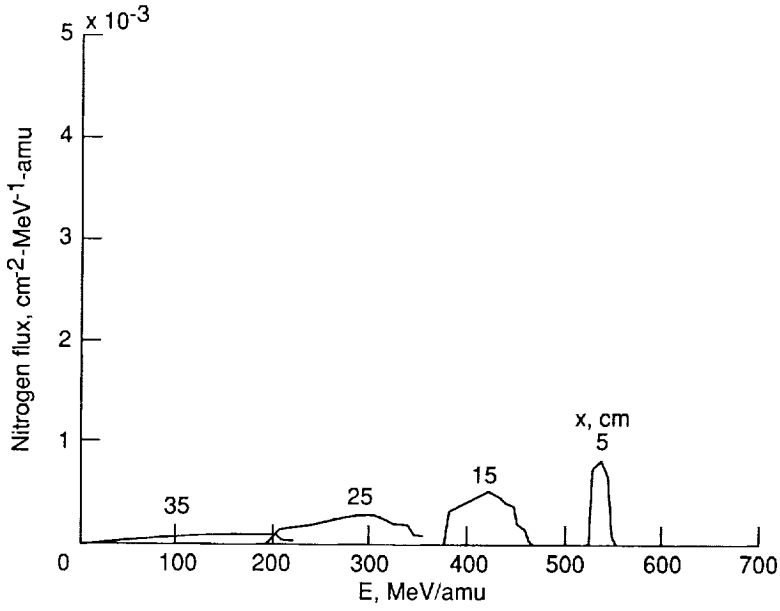

Figure 3.3. Nitrogen flux spectrum produced by a ^{20}Ne beam at 600 MeV/amu in a water column at various depths.

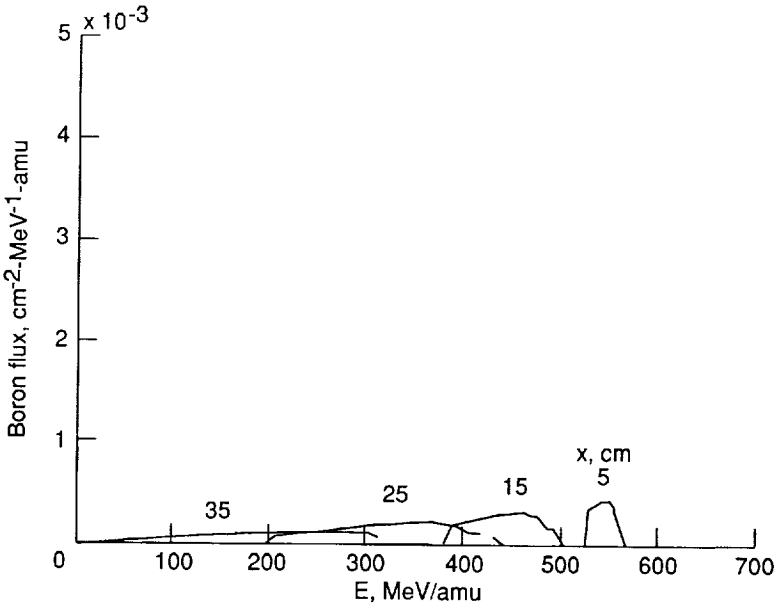

Figure 3.4. Boron flux spectrum produced by a ^{20}Ne beam at 600 MeV/amu in a water column at various depths.

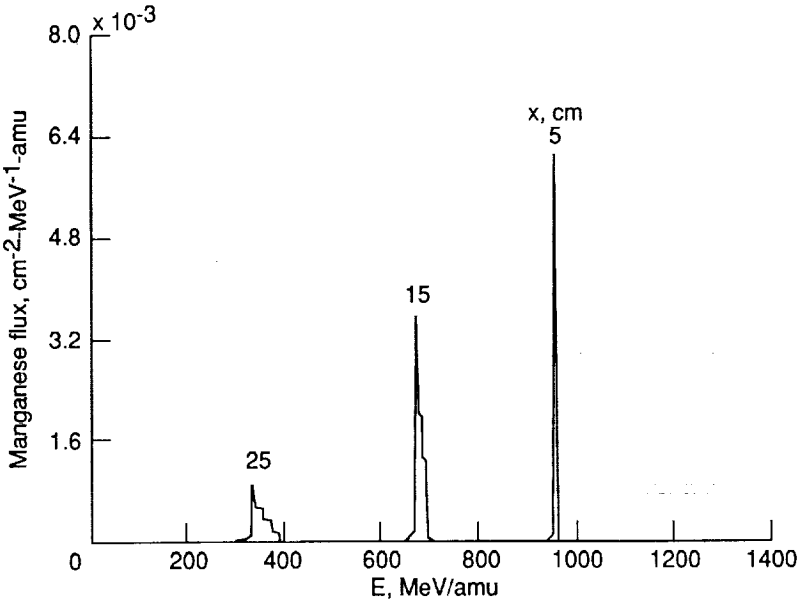

Figure 3.5. Manganese flux spectrum produced by a ^{56}Fe beam at 1090 MeV/amu in a water column at various depths.

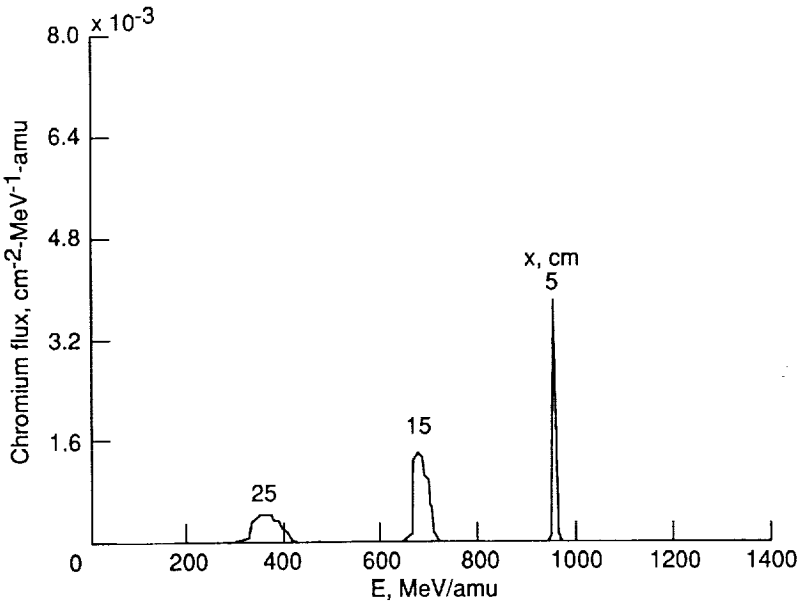

Figure 3.6. Chromium flux spectrum produced by a ^{56}Fe beam at 1090 MeV/amu in a water column at various depths.

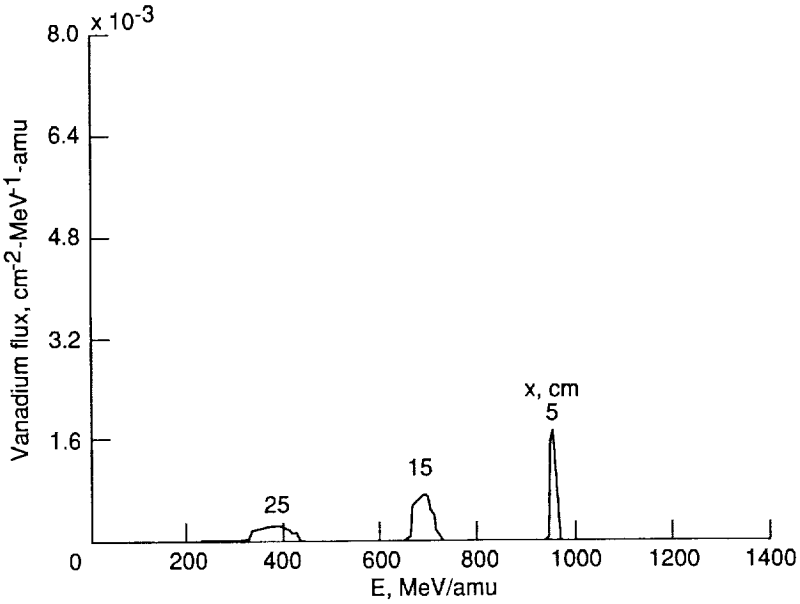

Figure 3.7. Vanadium flux spectrum produced by a ^{56}Fe beam at 1090 MeV/amu in a water column at various depths.

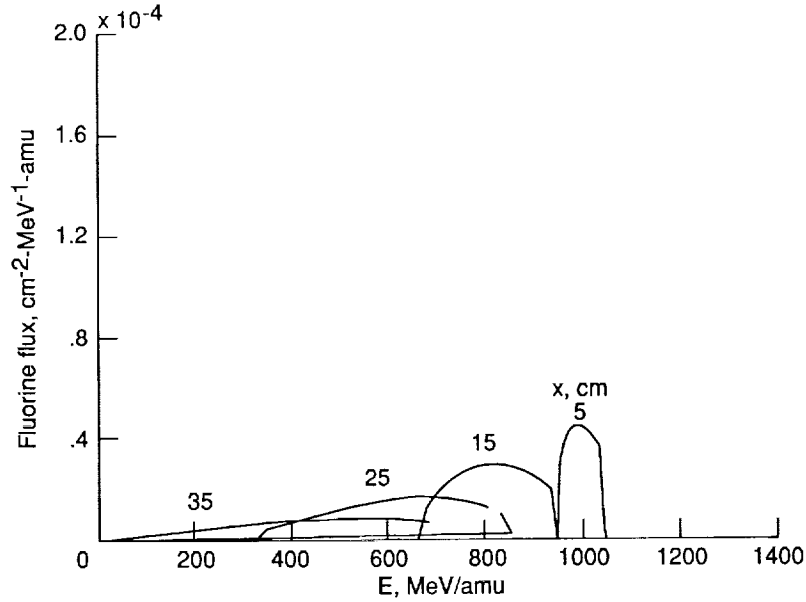

Figure 3.8. Fluorine flux spectrum produced by a ^{56}Fe beam at 1090 MeV/amu in a water column at various depths.

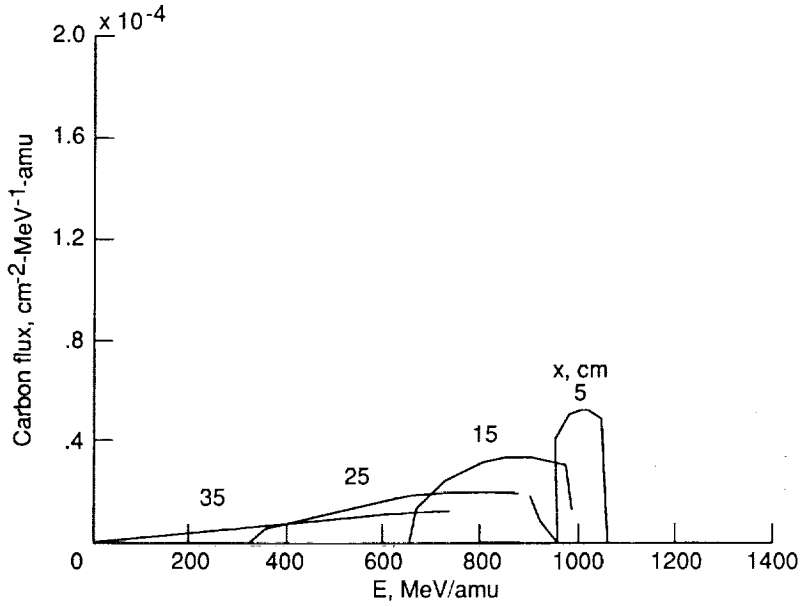

Figure 3.9. Carbon flux spectrum produced by a ^{56}Fe beam at 1090 MeV/amu in a water column at various depths.

4. Realistic Ion Beams

In the previous section, we assumed that a monoenergetic beam was present at the boundary. We now take the incident ion beam flux to be

$$\phi_j(0,E) = \frac{1}{\sqrt{2\pi}\Delta} \exp\left[-\frac{(E-E_o)^2}{2\Delta^2}\right] \tag{4.1}$$

where E_o is the nominal beam energy and Δ is related to the half-width at half-maximum. The full solution is then found as a superposition of results from the previous section. The uncollided flux is found to be

$$\phi_M^{(0)}(x,E) = \frac{\tilde{S}_M(E_m)}{\tilde{S}_M(E)} \exp(-\sigma_M x) \frac{1}{\sqrt{2\pi}\Delta} \exp\left[\frac{(E_o-E_m)^2}{2\Delta^2}\right] \tag{4.2}$$

where $R_M(E_m) = R_M(E) + x$. One similarly arrives at

$$\phi_j^{(1)}(x,E) = \frac{\sigma_{jM}\nu_j}{\tilde{S}_j(E)\,|\nu_M - \nu_j|} \exp\left\{-\frac{1}{2}\sigma_j\left[x - R_j(E) - \eta_o'\right] - \frac{1}{2}\sigma_M\left[x + R_j(E) + \eta_o'\right]\right\}$$
$$\times \frac{1}{2}\left[\mathrm{erf}\left(\frac{E_u - E_o}{\sqrt{2}\Delta}\right) - \mathrm{erf}\left(\frac{E_l - E_o}{\sqrt{2}\Delta}\right)\right] \tag{4.3}$$

where

$$E_l = R_M^{-1}\left\{\frac{\nu_j}{\nu_M}\left[R_j(E) + x\right]\right\} \tag{4.4}$$

$$E_u = R_M^{-1}\left\{\frac{\nu_j}{\nu_M}\left[R_j(E) + x\right]\right\} \tag{4.5}$$

$$\eta_o' = \frac{2\nu_M}{\nu_M - \nu_j} R_M(E_o) - \frac{\nu_M + \nu_j}{\nu_M - \nu_j}\left[R_j(E) + x\right] \tag{4.6}$$

The second collision contribution to the ion energy spectrum is similar:

$$\phi_j^{(2)}(x,E) = \sum_k \frac{\sigma_{jk}\sigma_{kM}\nu_j}{\widetilde{S}_j(E)\,|\nu_M - \nu_k|\,\Delta_{jkM}} \left[\exp(\sigma_M x_{Ml} - \sigma_k x_{kl} - \sigma_j x_{jl})\right.$$
$$\left. - \exp(-\sigma_M x_{Mu} - \sigma_k x_{ku} - \sigma_j x_{ju})\right]$$
$$\times \frac{1}{2}\left[\mathrm{erf}\left(\frac{E_u - E_o}{\sqrt{2}\Delta}\right) - \mathrm{erf}\left(\frac{E_l - E_o}{\sqrt{2}\Delta}\right)\right] \tag{4.7}$$

where

$$E_l = \left\{ \begin{array}{ll} R_M^{-1}\left[\dfrac{\nu_k R_k(E) + \nu_j x}{\nu_M}\right] & (\nu_M > \nu_k > \nu_j) \\ R_M^{-1}\left[\dfrac{R_M(E) + \nu_j x}{\nu_M}\right] & (\nu_k > \nu_M > \nu_j) \\ R_M^{-1}\left[\dfrac{\nu_k(R_k(E) + x)}{\nu_M}\right] & (\nu_M > \nu_j > \nu_k) \end{array} \right\} \tag{4.8}$$

$$E_u = \left\{ \begin{array}{ll} R_M^{-1}\left[R_M(E) + x\right] & (\nu_M > \nu_k > \nu_j) \\ R_M^{-1}\left[\dfrac{\nu_k(R_k(E) + x)}{\nu_M}\right] & (\nu_k > \nu_M > \nu_j) \\ R_M^{-1}\left[R_M(E) + x\right] & (\nu_M > \nu_j > \nu_k) \end{array} \right\} \tag{4.9}$$

and x_M and x_k evaluated at the upper and lower limit values of x_j are obtained from equations (3.31) and (3.32).

The elemental flux spectra were recalculated for ^{20}Ne ions at 600 MeV/amu with a 0.2-percent energy spread assumed for the primary beam. The resulting fluorine flux is shown in figure 4.1. Although the spectral results are quite similar to the monoenergetic beam case, there is a considerable smoothing of the total spectrum. Similar results are obtained for the oxygen flux as well in figure 4.2. In distinction, the nitrogen and carbon spectra show only slight isotopic structure as seen in figures 4.3 and 4.4. Qualitatively similar results are obtained for the ^{56}Fe realistic beam as shown in figures 4.5 through 4.9.

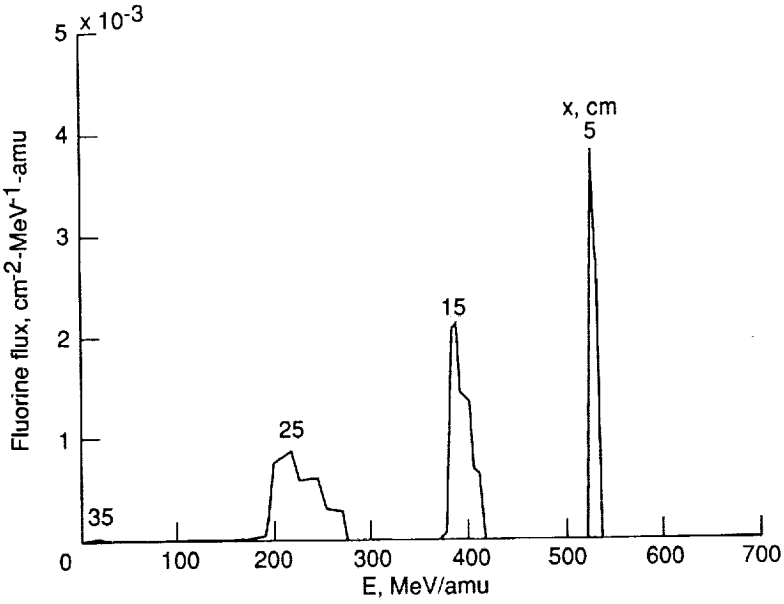

Figure 4.1. Fluorine flux spectrum produced by a ^{20}Ne beam at 600 MeV/amu with a 0.2-percent energy spread in a water column at various depths.

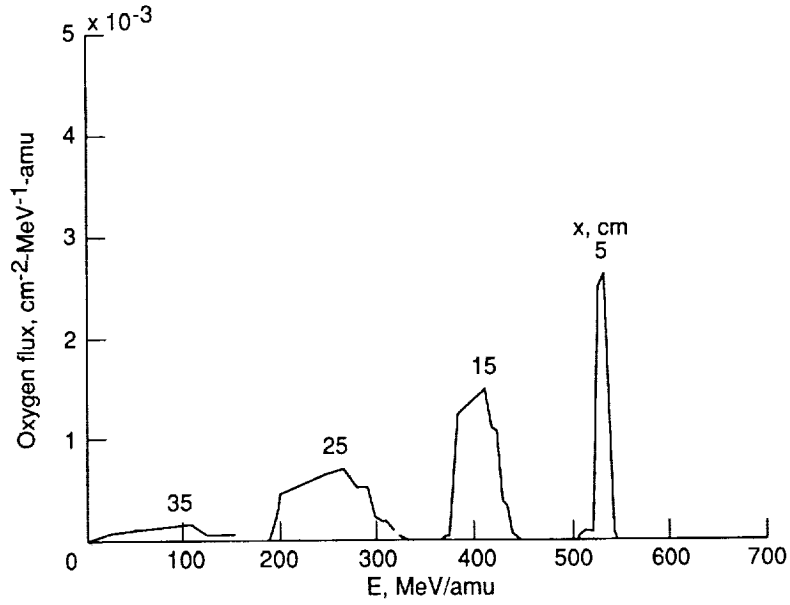

Figure 4.2. Oxygen flux spectrum produced by a ^{20}Ne beam at 600 MeV/amu with a 0.2-percent energy spread in a water column at various depths.

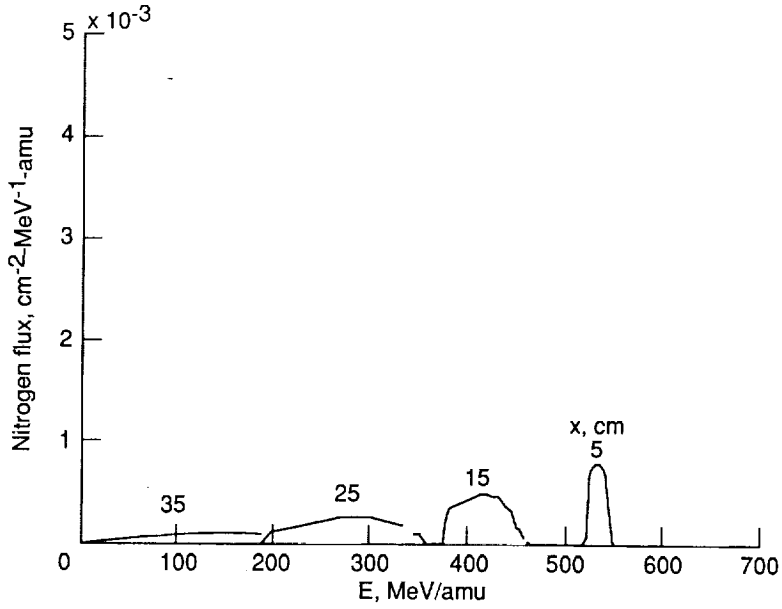

Figure 4.3. Nitrogen flux spectrum produced by a ^{20}Ne beam at 600 MeV/amu with a 0.2-percent energy spread in a water column at various depths.

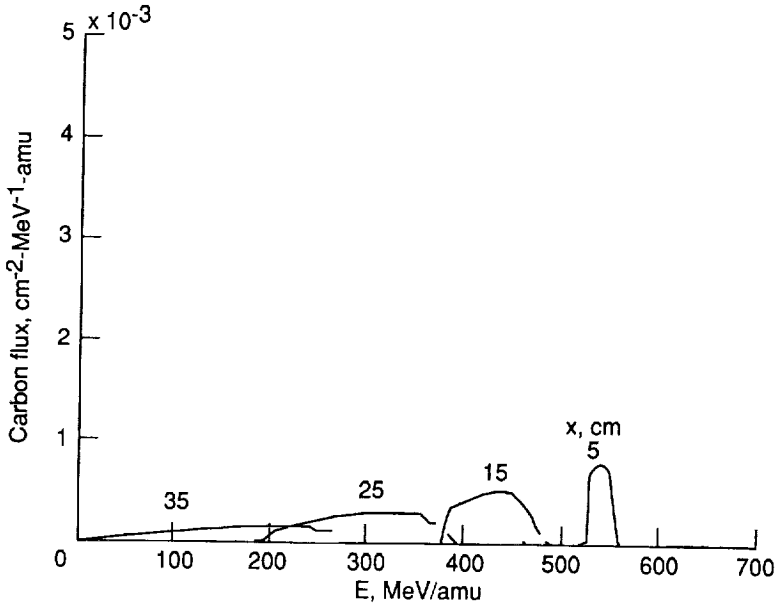

Figure 4.4. Carbon flux spectrum produced by a ^{20}Ne beam at 600 MeV/amu with a 0.2-percent energy spread in a water column at various depths.

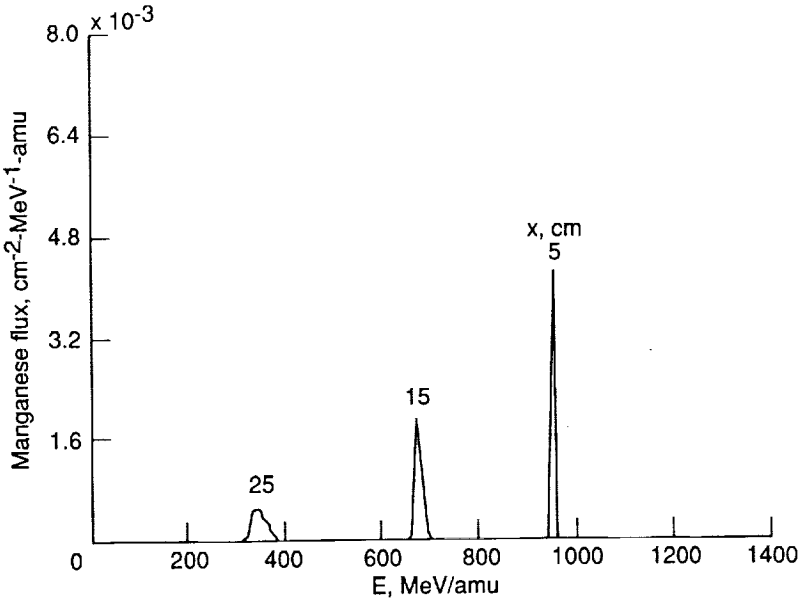

Figure 4.5. Manganese flux spectrum produced by a ^{56}Fe beam at 1090 MeV/amu with a 0.2-percent energy spread in a water column at various depths.

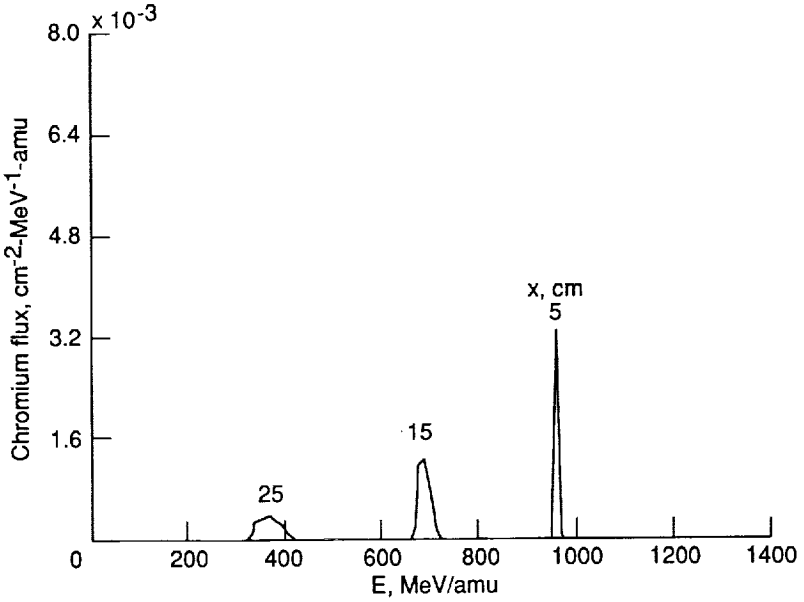

Figure 4.6. Chromium flux spectrum produced by a ^{56}Fe beam at 1090 MeV/amu with a 0.2-percent energy spread in a water column at various depths.

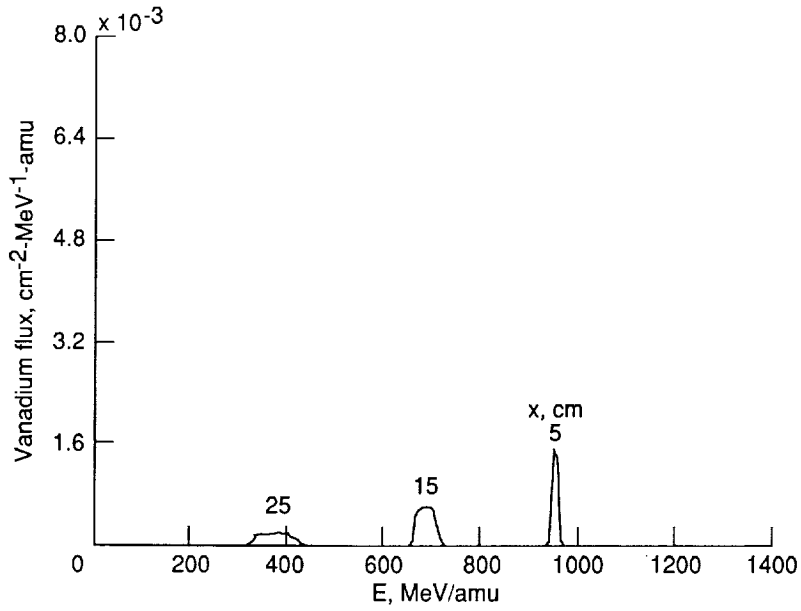

Figure 4.7. Vanadium flux spectrum produced by a ^{56}Fe beam at 1090 MeV/amu with a 0.2-percent energy spread in a water column at various depths.

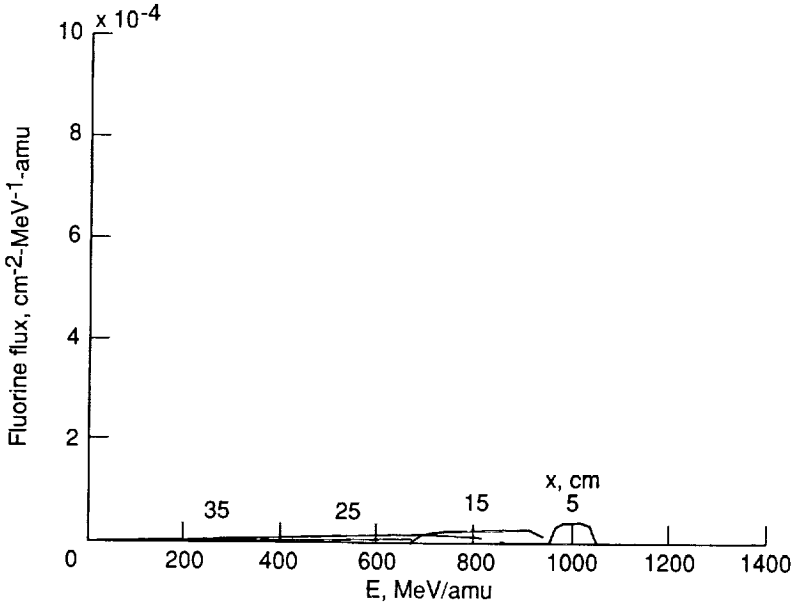

Figure 4.8. Fluorine flux spectrum produced by a ^{56}Fe beam at 1090 MeV/amu with a 0.2-percent energy spread in a water column at various depths.

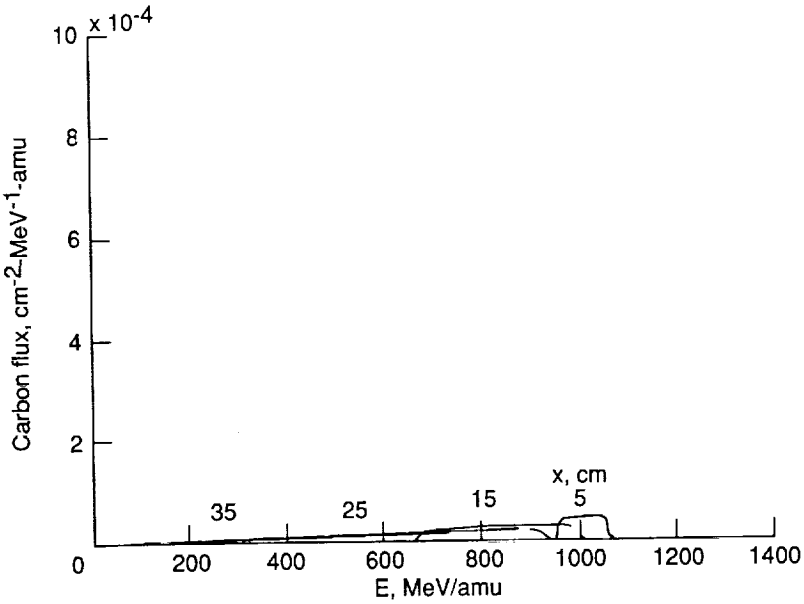

Figure 4.9. Carbon flux spectrum produced by a ^{56}Fe beam at 1090 MeV/amu with a 0.2-percent energy spread in a water column at various depths.

5. Approximate Spectral Solutions

In the previous sections, the spectral solutions of the secondary ion flux were derived to second-order collision terms. Such a three-term expansion is not always an adequate representation of the transport solution. In this section, we derive approximate expressions for the perturbation series. Clearly, the more accurate results would be used to the order to which they are known, and the higher order terms would be taken to the approximate expressions of this section.

5.1. Approximate Monoenergetic Beams

The uncollided beam solution is taken as

$$\phi_j^{(0)}(x,E) = \phi_j^{(0)}(x)\frac{1}{\tilde{S}_j(E)}\delta[x + R_j(E) - R_j(E_o)] \tag{5.1}$$

which is equal to the result in equation (3.27). The first-order collision term is approximated by noting that the energy dependence of the exponent of equation (3.28) is slowly varying in energy (refs. 4 through 7) resulting in

$$\phi_j^{(1)}(x,E) \approx \frac{\phi_j^{(1)}(x)}{E_{ju} - E_{jl}} \tag{5.2}$$

where

$$E_{jl} = R_j^{-1}\left\{\frac{\nu_M}{\nu_j}[R_M(E_o) - x]\right\} \tag{5.3}$$

$$E_{ju} = R_j^{-1}\left\{\frac{\nu_M}{\nu_j}R_M(E_o) - x\right\} \tag{5.4}$$

Similarly,

$$\phi_j^{(2)}(x,E) = \sum_k \frac{\sigma_{jk}\sigma_{kM}\ g(j,k,M)}{E_{ju} - E_{jl}} \tag{5.5}$$

where

$$E_{jl} = \left\{ \begin{array}{ll} R_M^{-1}\left\{R_M(E_o) - x\right\} & (\nu_M > \nu_k > \nu_j) \\ R_k^{-1}\left\{\dfrac{\nu_M}{\nu_k}\ R_M(E_o) - x\right\} & (\nu_k > \nu_M > \nu_j) \\ R_M^{-1}\left\{R_M(E_o) - x\right\} & (\nu_M > \nu_j > \nu_k) \end{array} \right\} \tag{5.6}$$

and

$$E_{ju} = \left\{ \begin{array}{ll} R_k^{-1}\left\{\dfrac{\nu_M\ R_M(E_o) - \nu_j x}{\nu_k}\right\} & (\nu_M > \nu_k > \nu_j) \\ R_M^{-1}\left\{\dfrac{R_M(E_o) - \nu_j x}{\nu_M}\ \right\} & (\nu_k > \nu_M > \nu_j) \\ R_k^{-1}\left\{\dfrac{\nu_M}{\nu_k}\ R_M(E_o) - x\right\} & (\nu_M > \nu_j > \nu_k) \end{array} \right\} \tag{5.7}$$

Higher order terms ($n > 2$) are taken as

$$\phi_j^n(x,E) \approx \frac{\phi_j^{(n)}(x)}{E_{ju} - E_{jl}} \tag{5.8}$$

where E_{ju} and E_{jl} are given by equations (5.6) and (5.7). In all the expressions for $\phi_j^{(n)}$ given by equations (5.2), (5.5), and (5.8), the flux values are taken as zero unless

$$E_{jl} \leq E \leq E_{ju} \tag{5.9}$$

The approximate monoenergetic beam solutions are given in figures 5.1 through 5.4 and should be compared with the solutions found in section 3. The ^{17}O flux at 20 cm of water is shown in figure 5.1 as contributed by the first collision term. The trapezoidal (solid) curve is the exact solution for the first collision term derived in section 3. The rectangular (dashed) curve is the approximate first collision term of equation (5.2). Terms for other fragment spectra are similar to those shown in figure 5.1. The solution for the second collision contribution to the ^{17}O flux at 20 cm of water is shown in figure 5.2. The nearly rectangular solution (dashed curve) is the approximation given by equation (5.5). A triangular spectral function of the same energy interval could yield improved results. The spectra of fragments which are much lighter than the primary beam are more accurately represented by the approximate solutions as seen in figures 5.3 and 5.4. This improvement results from the greater number of terms in the summation of equation (3.44). This leads us to believe that the higher order terms in the perturbation series can be adequately represented by the approximation in equation (5.8). This is especially true because higher order terms in many applications are only small corrections.

5.2. Approximate Realistic Beams

Approximate solutions for realistic ion beams may be found by using a superposition of the approximate monoenergetic beam solutions. The incident ion beam is taken as

$$\phi_j(0,E) = \frac{1}{\sqrt{2\pi}\Delta} \exp\left[-\frac{(E-E_o)^2}{2\Delta^2}\right] \delta_{jM} \tag{5.10}$$

where E_o is the nominal beam energy, and Δ is related to the half-width at half-maximum. The first term is then as before

$$\phi_M^{(0)}(x,E) = \frac{\tilde{S}_M(E_m)}{\tilde{S}_M(E)} \exp(-\sigma_M x) \frac{1}{\sqrt{2\pi}\Delta} \exp\left[-\frac{(E_o - E_m)^2}{2\Delta^2}\right] \tag{5.11}$$

where $R_M(E_m) = R_M(E) + x$. One similarly arrives at

$$\phi_j^{(1)}(x,E) = \phi_j^{(1)}(x)\frac{1}{2}\left[\mathrm{erf}\left(\frac{E_u - E_o}{\sqrt{2}\Delta}\right) - \mathrm{erf}\left(\frac{E_l - E_o}{\sqrt{2}\Delta}\right)\right](E_{ju} - E_{jl})^{-1} \tag{5.12}$$

where

$$E_u = R_M^{-1}\left\{\frac{\nu_j}{\nu_M}[R_j(E) + x]\right\} \tag{5.13}$$

$$E_l = R_M^{-1}\left\{\frac{\nu_j}{\nu_M}[R_j(E) + x]\right\} \tag{5.14}$$

and E_{ju} and E_{jl} are given by equations (5.3) and (5.4). Additional computation yields

$$\phi_j^{(2)}(x,E) = \sum_k \frac{\sigma_{jk}\sigma_{kM}\, g(j,k,M)\left\{\mathrm{erf}\left[(E_u - E_o)/\sqrt{2}\Delta - \mathrm{erf}(E_l - E_o)/\sqrt{2}\Delta\right]\right\}}{2(E_{ju} - E_{jl})} \tag{5.15}$$

where E_{ju} and E_{jl} are given by equations (5.6) and (5.7), and E_l and E_u are given in equations (4.8) and (4.9). The remaining higher order terms are taken as

$$\phi_j^{(n)}(x,E) = \sum_{j_1,\ldots,j_{n-1}} \frac{\sigma_{jj_{n-1}},\ldots,\sigma_{j1},M\; g(j,j_{n-1},\ldots,j_1,M)\;\mathrm{erf}\left[(E_u - E_o)/\sqrt{2}\Delta\right] - \mathrm{erf}\left[(E_1 - E_o)/\sqrt{2}\Delta\right]}{2(E_{ju} - E_{jl})} \tag{5.16}$$

where E_{jl} and E_{ju} are given by equations (5.2) and (5.3) and E_u and E_l are given by equations (5.13) and (5.14).

These approximate equations for realistic ion beams are given in figures 5.5 to 5.8 and should be compared with the more exact formulae given in section 4. The primary ion beam is taken as ^{20}Ne at 600 MeV/amu with a 0.2-percent energy spread. The ^{17}O flux first collision term is shown in figure 5.5 for the two formalisms. The effect of the beam energy spread is seen as a rounding of the spectrum at the edges compared with the monoenergetic case in figure 5.1. The second collision term is shown in figure 5.6. The approximate second collision term improves for the lighter fragments as seen in figures 5.7 and 5.8. Higher order collision terms are expected to be more accurate because of the large number of combinations of contributing ion terms.

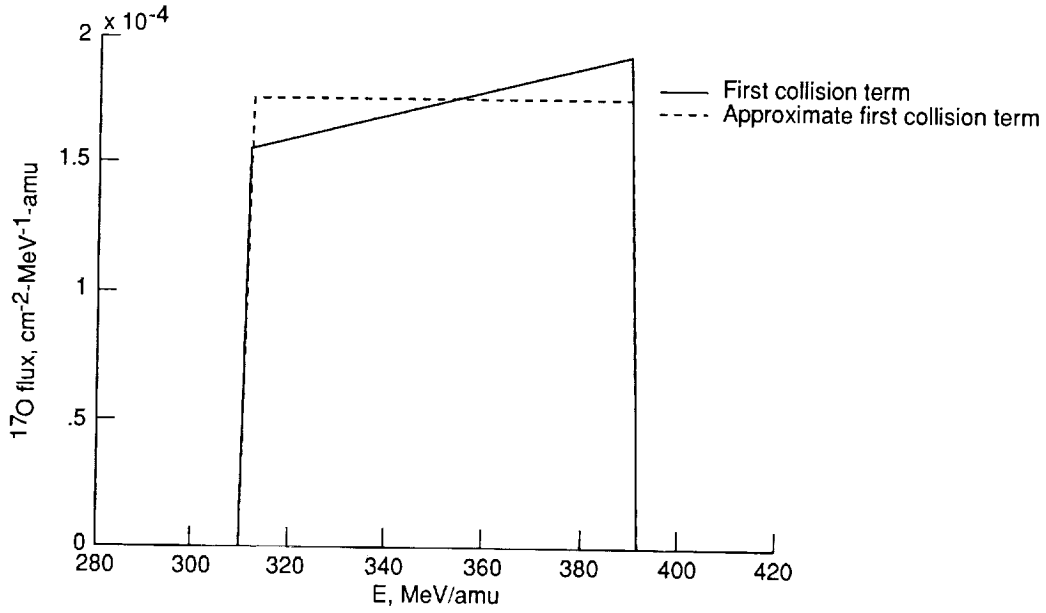

Figure 5.1. ^{17}O flux spectral term according to first collision term and approximate first collision term.

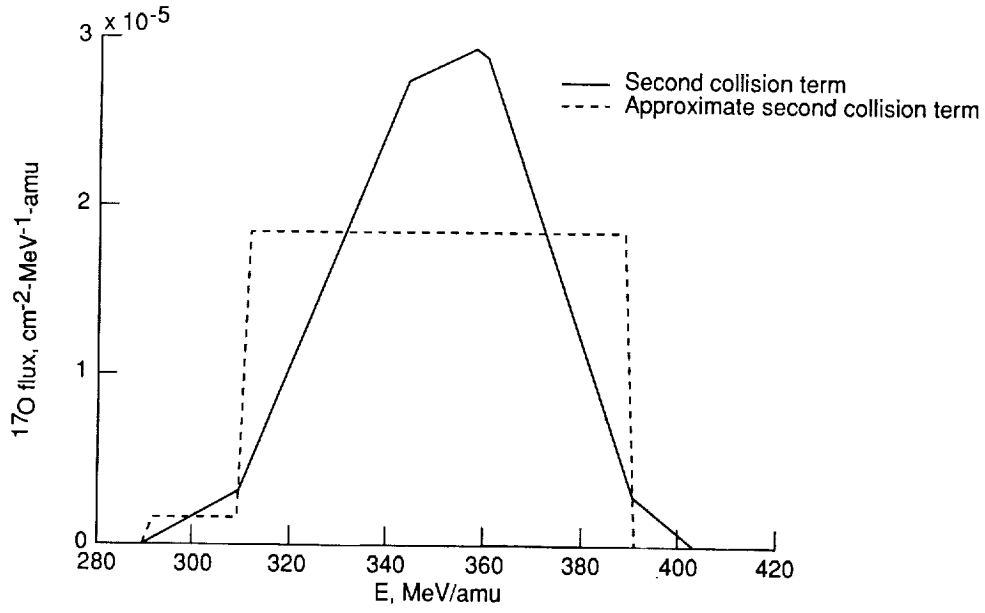

Figure 5.2. ^{17}O flux spectral term according to second collision term and approximate second collision term.

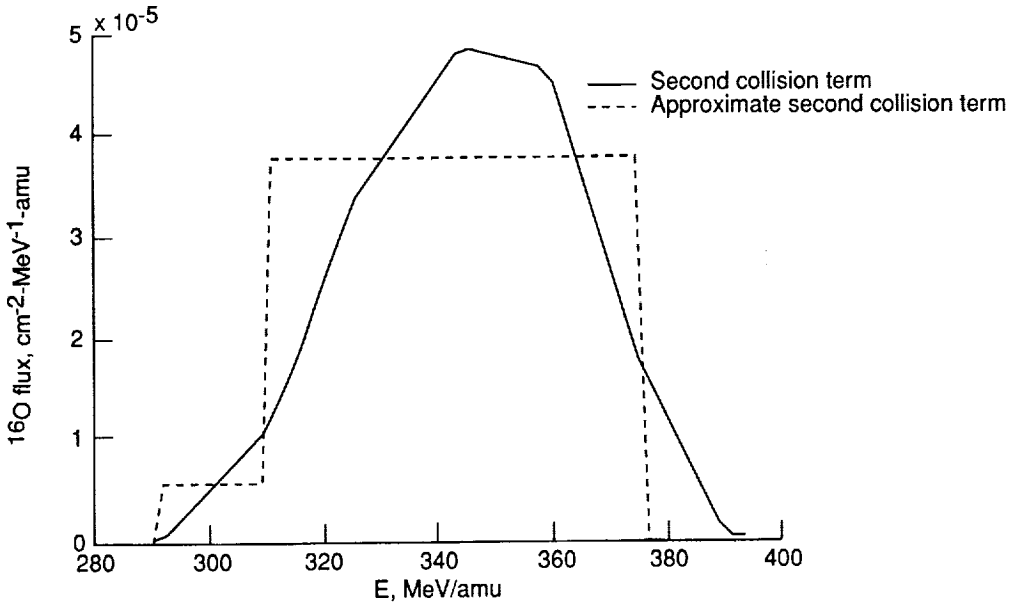

Figure 5.3. ^{16}O flux spectral term according to second collision term and approximate second collision term.

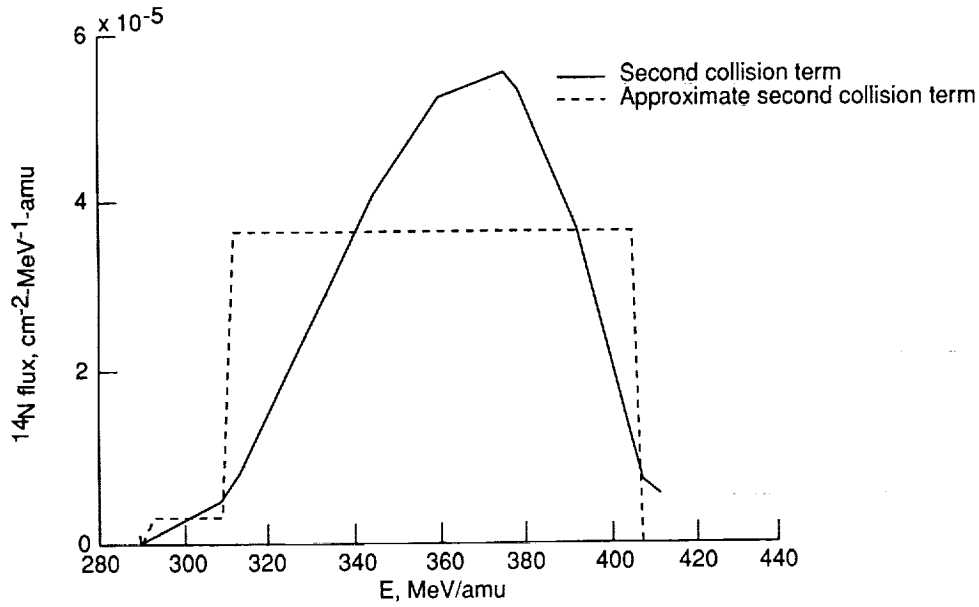

Figure 5.4. ^{14}N flux spectral term according to second collision term and approximate second collision term.

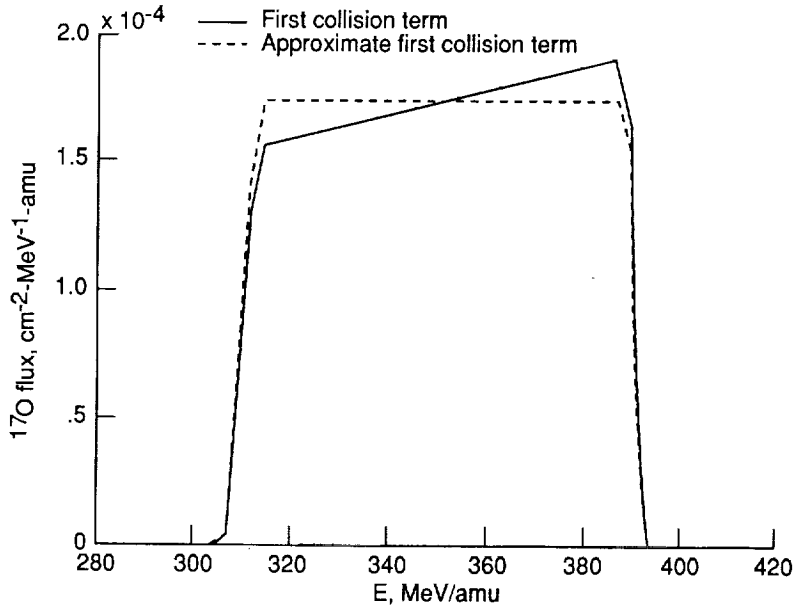

Figure 5.5. ^{17}O flux spectral term for energy spread ^{20}Ne beam according to first collision term and approximate first collision term.

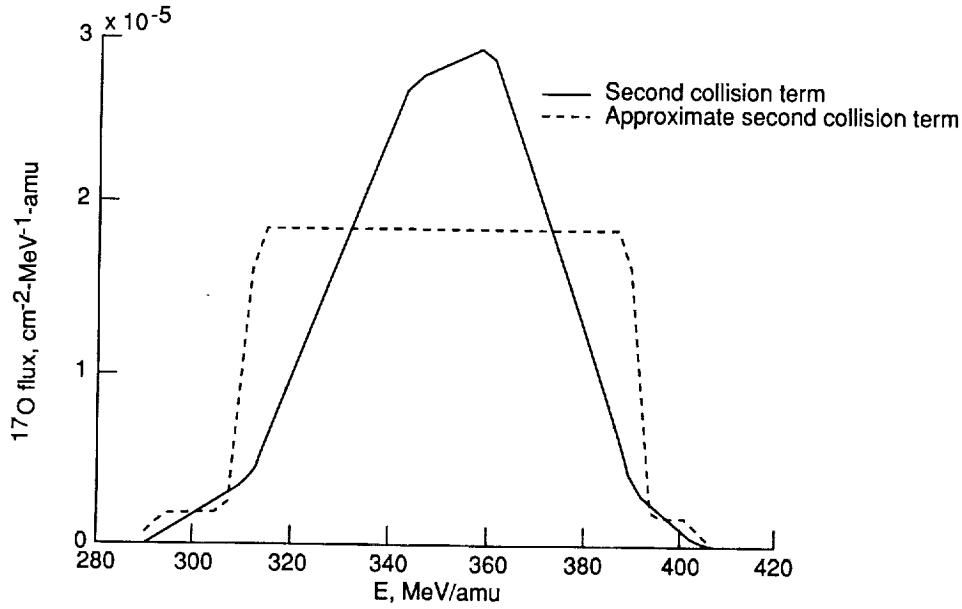

Figure 5.6. ^{17}O flux spectral term for energy spread ^{20}Ne beam according to second collision term and approximate second collision term.

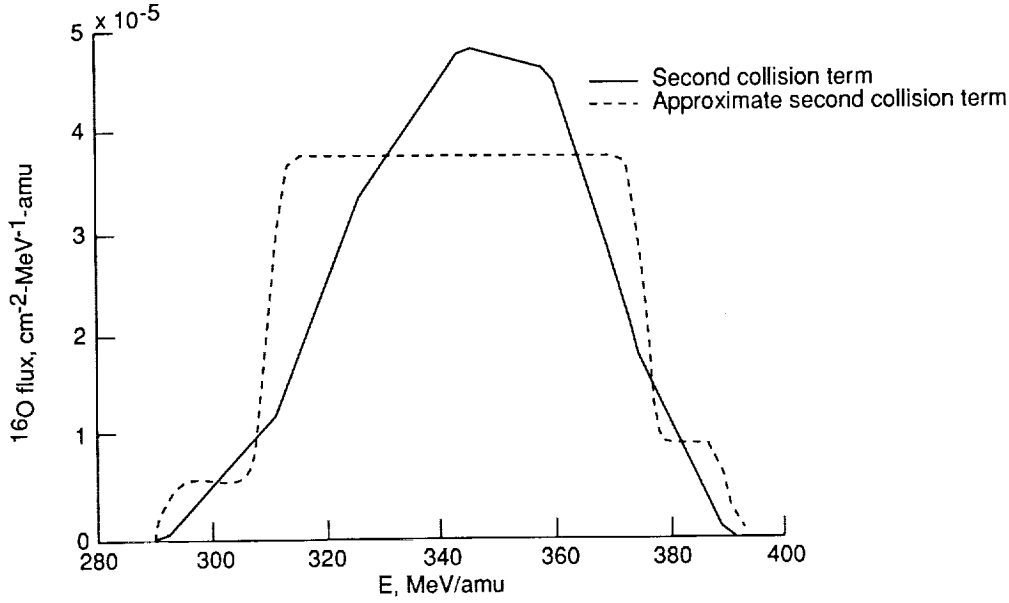

Figure 5.7. ^{16}O flux spectral term for energy spread ^{20}Ne beam according to second collision term and approximate second collision term.

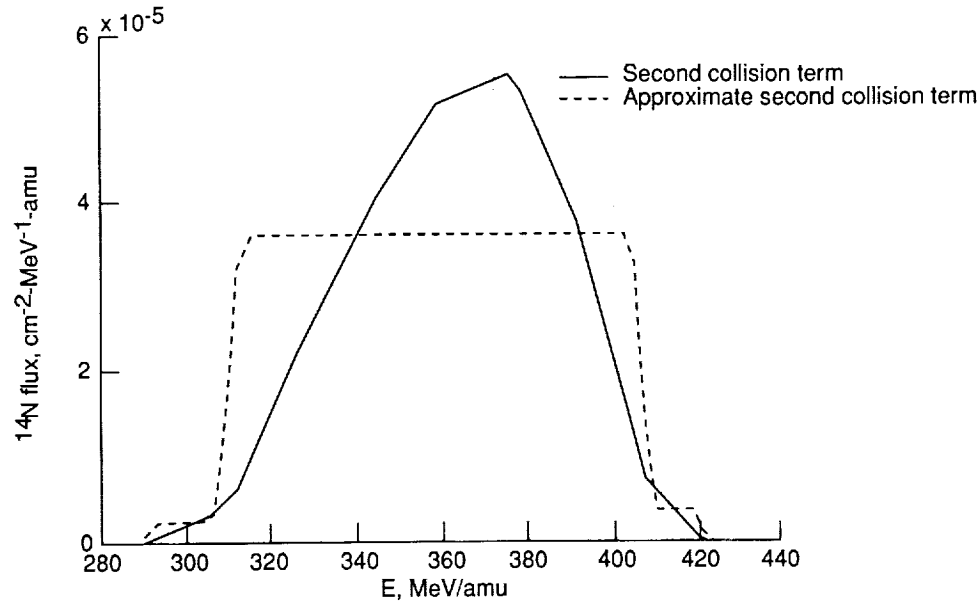

Figure 5.8. ^{14}N flux spectral term for energy spread ^{20}Ne beam according to second collision term and approximate second collision term.

6. Recommended Methods

An energy-independent theory has been used to show that the perturbation expansion up to the double collision term is adequate for all fragments whose mass is near that of the projectile. This is why the three-term expansion was able to explain the Bragg curve data for ^{20}Ne beams in water with reasonable accuracy (ref. 7). As a starting point for the calculation of the transition of heavy ion beams in materials, the use of the three-term expansion of sections 3 and 4 can be further corrected by use of the approximate higher order terms given in section 5. As an example of such a procedure, we give results for ^{20}Ne beams at 600 MeV/amu in water. The results are shown in figures 6.1 to 6.6 as successive partial sums of the perturbation series. The solid line is the first collision term. The dashed curve includes the double collision terms. The long-dash–short-dash curve includes the triple collision term and can hardly be distinguished from the long-dash–double-short-dash curve which includes the quadruple collision terms. The results for penetration to 20 cm of water are shown in figures 6.1 to 6.6. The monoenergetic beam results for ^{17}O, ^{16}O, and ^{12}C are given in figures 6.1 to 6.3, respectively. The double collision term is seen to be always an important contribution. The triple collision term shows some importance for ^{12}C, while higher order terms are negligible. Similar results are shown in figures 6.4 to 6.6 for an energy spread of 0.2 percent.

NASA Langley Research Center
Hampton, VA 23665-5225
May 11, 1989

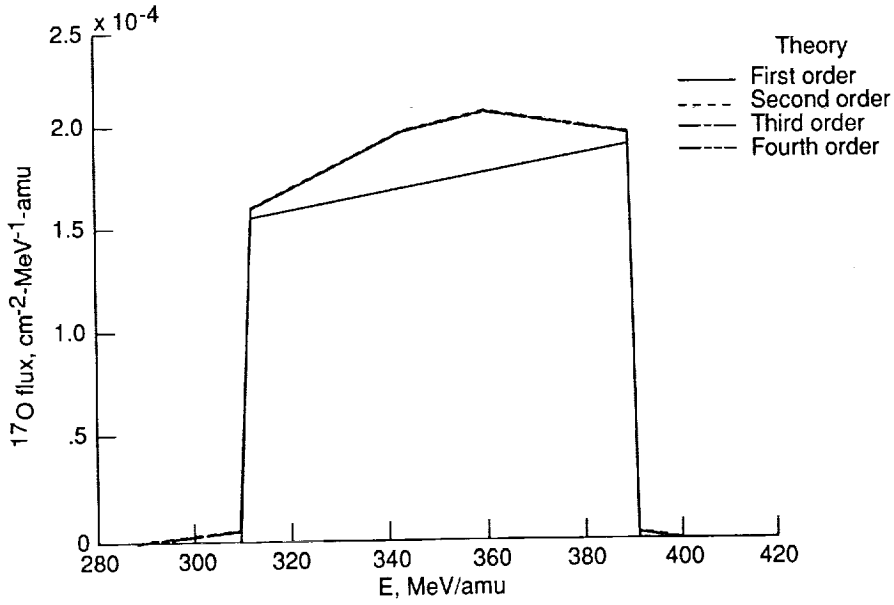

Figure 6.1. Sequence of approximations of ^{17}O flux spectrum after 20 cm of water for first-order, second-order, third-order, and fourth-order theories.

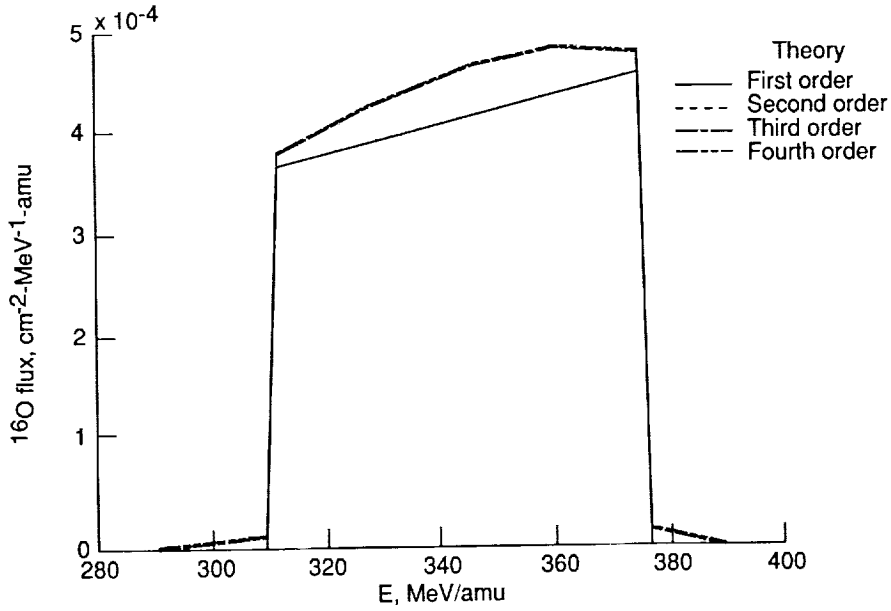

Figure 6.2. Sequence of approximations of ^{16}O flux spectrum after 20 cm of water for first-order, second-order, third-order, and fourth-order theories.

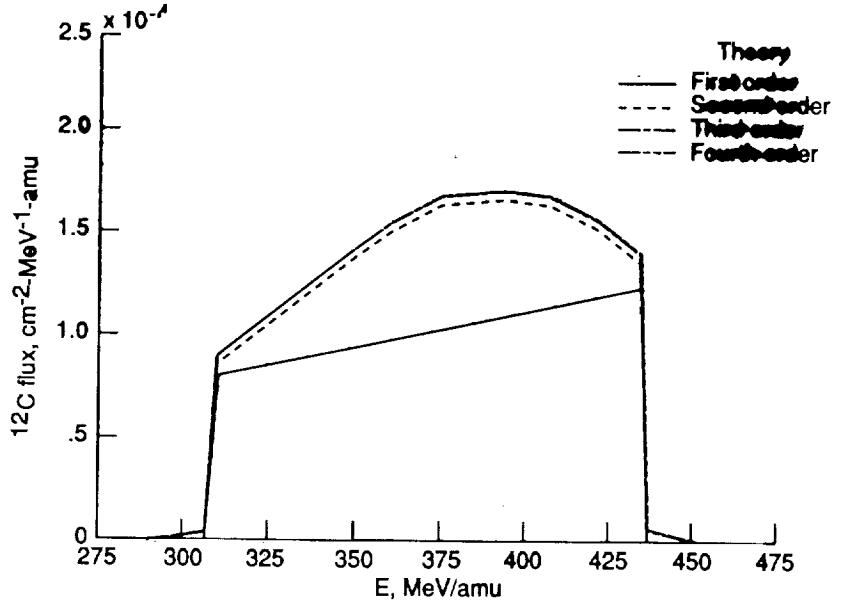

Figure 6.3. Sequence of approximations of ^{12}C flux spectrum after 20 cm of water for first-order, second-order, third-order, and fourth-order theories.

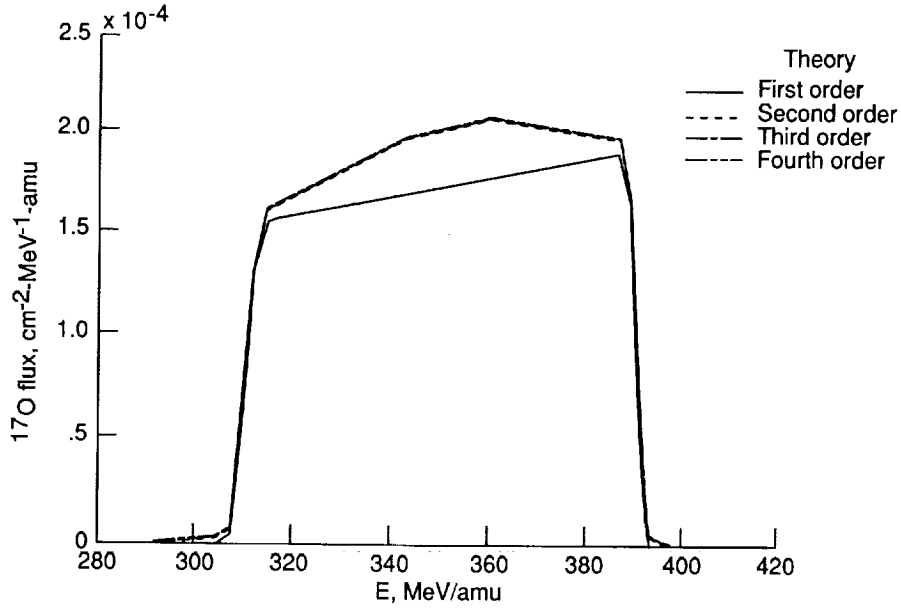

Figure 6.4. Sequence of approximations for energy spread solution of ^{17}O flux spectrum after 20 cm of water for first-order, second-order, third-order, and fourth-order theories.

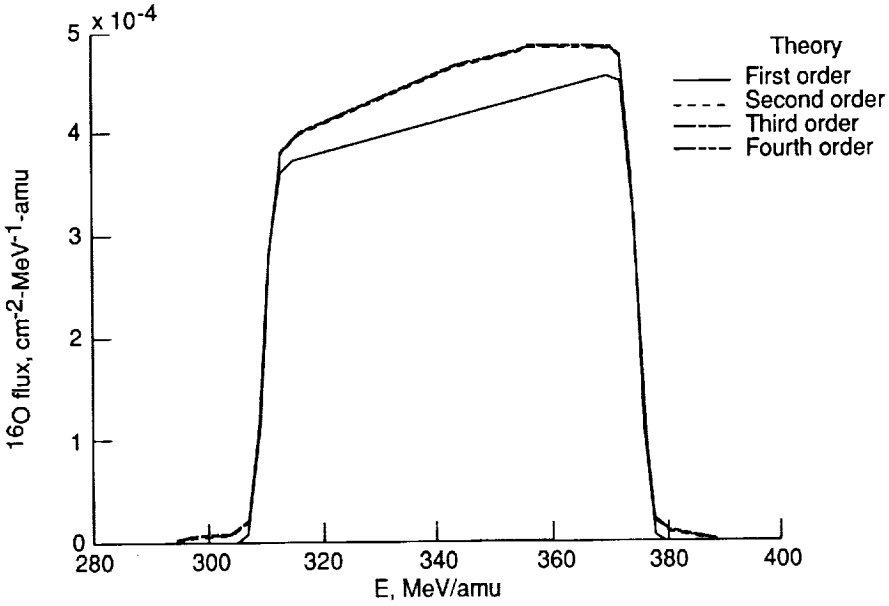

Figure 6.5. Sequence of approximations for energy spread solution of ^{16}O flux spectrum after 20 cm of water for first-order, second-order, third-order, and fourth-order theories.

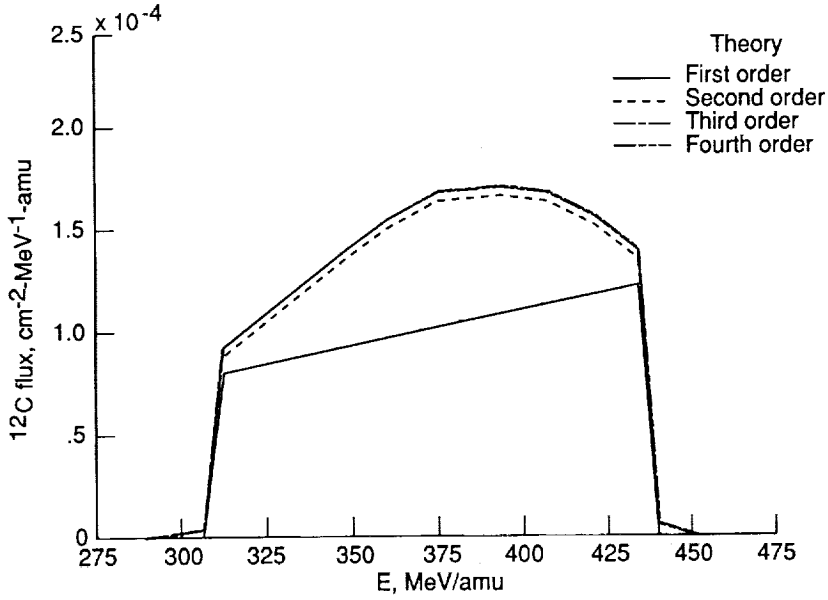

Figure 6.6. Sequence of approximations for energy spread solution of ^{12}C flux spectrum after 20 cm of water for first-order, second-order, third-order, and fourth-order theories.

References

1. Wilson, John W.; and Badavi, F. F.: Methods of Galactic Heavy Ion Transport. *Radiat. Res.*, vol. 108, 1986, pp. 231–237.
2. Wilson, J. W.; Townsend, L. W.; and Badavi, F. F.: Galactic HZE Propagation Through the Earth's Atmosphere. *Radiat. Res.*, vol. 109, no. 2, Feb. 1987, pp. 173–183.
3. Wilson, John W.; and Townsend, Lawrence W.: A Benchmark for Galactic Cosmic-Ray Transport Codes. *Radiat. Res.*, vol. 114, 1988, pp. 201–206.
4. Wilson, J. W.: Depth-Dose Relations for Heavy Ion Beams. *Virginia J. Sci.*, vol. 28, no. 3, 1977, pp. 136–138.
5. Wilson, John W.: *Analysis of the Theory of High-Energy Ion Transport.* NASA TN D-8381, 1977.
6. Wilson, John W.: *Heavy Ion Transport in the Straight Ahead Approximation.* NASA TP-2178, 1983.
7. Wilson, John W.; Townsend, L. W.; Bidasaria, H. B.; Schimmerling, Walter; Wong, Mervyn; and Howard, Jerry: ^{20}Ne Depth-Dose Relations in Water. *Health Phys.*, vol. 46, no. 5, May 1984, pp. 1101–1111.
8. Ganapol, Barry D.; Townsend, Lawrence W.; and Wilson, John W.: *Benchmark Solutions for the Galactic Ion Transport Equations: Energy and Spatially Dependent Problems.* NASA TP-2878, 1989.
9. Townsend, L. W.; and Wilson, J. W.: Nuclear Cross Sections for Hadronic Transport. *Trans. American Nucl. Soc.*, vol. 56, 1988, pp. 277–279.
10. Shavers, Mark R.: Heavy-Ion Transport Code Calculations and Comparison With Experiment for a 670A MeV Accelerated Neon Beam Interacting With Water. M.E. Thesis, Univ. of Florida, 1988.
11. Ziegler, J. F.; Biersack, J. P.; and Littmark, U.: The Stopping and Range of Ions in Solids. Volume 1 of *The Stopping and Ranges of Ions in Matter,* J. F. Ziegler, ed., Pergamon Press Inc., c.1985.
12. Andersen, H. H.: Bibliography and Index of Experimental Range and Stopping Power Data. Volume 2 of *The Stopping and Ranges of Ions in Matter,* J. F. Ziegler, organizer, Pergamon Press Inc., c.1977.
13. Andersen, H. H.; and Ziegler, J. F.: Hydrogen—Stopping Powers and Ranges in All Elements. Volume 3 of *The Stopping and Ranges of Ions in Matter,* J. F. Ziegler, organizer, Pergamon Press Inc., c.1977.
14. Ziegler, J. F.: Helium—Stopping Powers and Ranges in All Elemental Matter. Volume 4 of *The Stopping and Ranges of Ions in Matter,* J. F. Ziegler, organizer, Pergamon Press Inc., c.1977.
15. Ziegler, J. F.: Handbook of Stopping Cross-Sections for Energetic Ions in All Elements. Volume 5 of *The Stopping and Ranges of Ions in Matter,* J. F. Ziegler, ed., Pergamon Press Inc., c.1980.
16. Littmark, U.; and Ziegler, J. F.: Handbook of Range Distributions for Energetic Ions in All Elements. Volume 6 of *The Stopping and Ranges of Ions in Matter,* J. F. Ziegler, ed., Pergamon Press Inc., c.1980.

NASA
National Aeronautics and Space Administration

Report Documentation Page

1. Report No.	2. Government Accession No.	3. Recipient's Catalog No.
NASA TM-4118		

4. Title and Subtitle	5. Report Date
A Hierarchy of Transport Approximations for High Energy Heavy (HZE) Ions	July 1989
	6. Performing Organization Code
7. Author(s)	8. Performing Organization Report No.
John W. Wilson, Stanley L. Lamkin, Hamidullah Farhat, Barry D. Ganapol, and Lawrence W. Townsend	L-16572
9. Performing Organization Name and Address	10. Work Unit No.
NASA Langley Research Center Hampton, VA 23665-5225	199-22-76-01
	11. Contract or Grant No.
12. Sponsoring Agency Name and Address	13. Type of Report and Period Covered
National Aeronautics and Space Administration Washington, DC 20546-0001	Technical Memorandum
	14. Sponsoring Agency Code

15. Supplementary Notes

John W. Wilson and Lawrence W. Townsend: Langley Research Center, Hampton, Virginia.
Stanley L. Lamkin: PRC Kentron, Inc., Aerospace Technologies Division, Hampton, Virginia.
Hamidullah Farhat: Hampton University, Hampton, Virginia.
Barry D. Ganapol: University of Arizona, Tucson, Arizona.

16. Abstract

The transport of high energy heavy (HZE) ions through bulk materials is studied with energy dependence of the nuclear cross sections being neglected. A three-term perturbation expansion appears to be adequate for most practical applications for which penetration depths are less than 30 g/cm^2 of material. The differential energy flux is found for monoenergetic beams and for realistic ion beam spectral distributions. An approximate formalism is given to estimate higher order terms.

17. Key Words (Suggested by Authors(s))	18. Distribution Statement
Nuclear reactions Heavy ions Transport theory	Unclassified–Unlimited Subject Category 93

19. Security Classif. (of this report)	20. Security Classif. (of this page)	21. No. of Pages	22. Price
Unclassified	Unclassified	37	A03

NASA FORM 1626 OCT 86

NASA-Langley, 1989

For sale by the National Technical Information Service, Springfield, Virginia 22161-2171